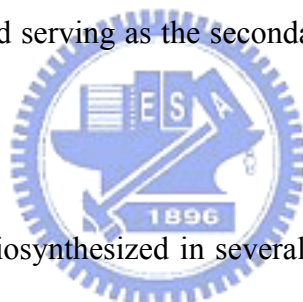


Chapter 1 Introduction and Background

1.1 Sterol

Sterols, biosynthesized via the cytoplasmic mevalonate (MVA) pathway, are important structural components of the plasma membrane and precursors of steroid in both vertebrates and plants. Four interconnected rings consist of carbon atoms with a hydroxyl group in the 3-position of the A-ring are the skeletal structure of steroids (Fig. 1-1). The hydroxyl group on the A ring is polar but the rest of the aliphatic chain is non-polar. Sterols are essential membrane constituents in eukaryotes. For example, cholesterol (Fig. 1-2) in cell membrane play an important role in maintaining the fluidity of the lipid bilayer and serving as the secondary messenger in developmental signaling.



Steroidal backbones are biosynthesized in several steps from acetyl-CoA: (a) the conversion of acetyl-CoA into acetoacetyl-CoA by acetoacetyl-CoA thiolase (AACT); (b) the conversion of acetoacetyl-CoA into 3-hydroxy-3-methylglutaryl-CoA by 3-hydroxy-3-methylglutaryl-CoA synthase (HMGS); (c) the conversion of 3-hydroxy-3-methylglutaryl-CoA into mevalonate by the key enzyme, 3-hydroxy-3-methylglutaryl-CoA reductase (HMGR); (d) the conversion of MVA into phosphomevalonate by mevalonate kinase (MK); (e) the conversion of phosphomevalonate into diphosphomevalonate by phosphomevalonate kinase (PMK); (f) the conversion of diphosphomevalonate into isopentenyl diphosphate (IPP) by mevalonate diphosphate decarboxyase (MVD); (g) the isomerization of IPP to dimethylallyl diphosphate (DMAPP) by IPP isomerase (IPI); (h) the condensation of DMAPP with IPP to form geranyl diphosphate (GPP) by geranyl diphosphate synthase

(GPS); (i) the condensation of GPP with IPP to form farnesyl diphosphate by farnesyl diphosphate synthase (FPS); (j) the condensation of two farnesyl diphosphate molecules to form squalene by squalene synthase (SQS); (k) the oxidation of squalene to 2,3-oxidosqualene (OS) by squalene epoxidase (SQE); and (l) the cyclization of OS into lanosterol or cycloartenol by lanosterol synthase (LAS) and cycloartenol synthase (CAS), respectively¹. After a serial cyclization and/or rearrangement cascades, the formation of the triterpenoids with diverse structure is dependent on the species. As shown in Fig. 1-3.

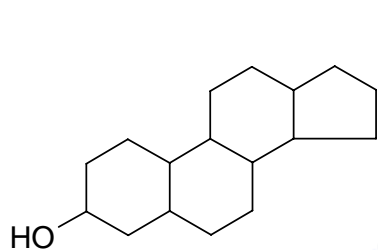


Fig 1-1. Sterol backbone

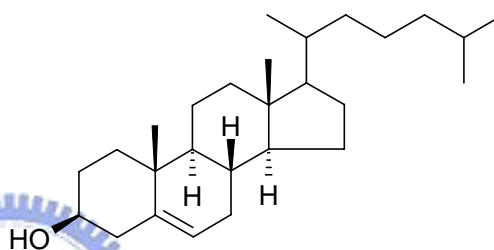


Fig. 1-2. Cholesterol

Sterol Biosynthetic Pathway

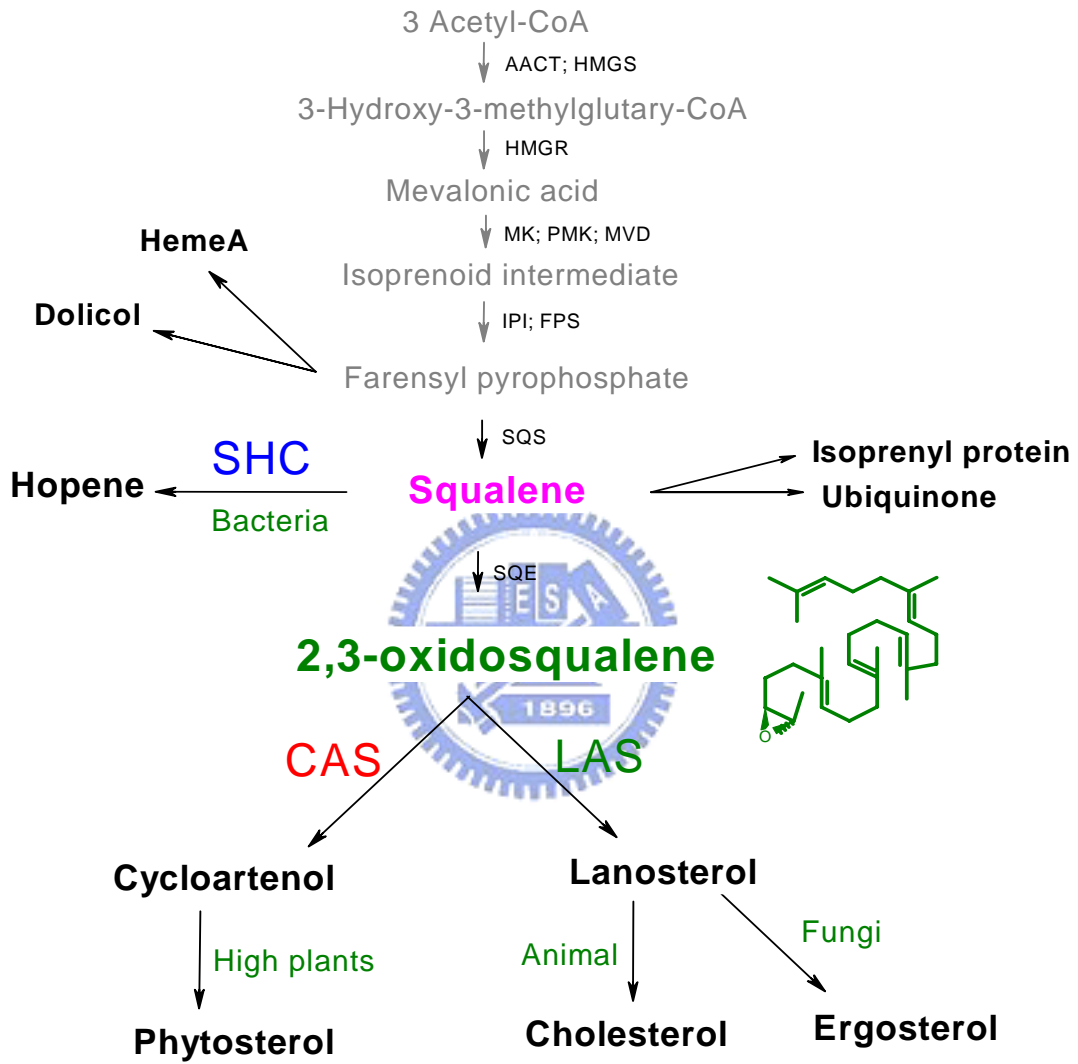
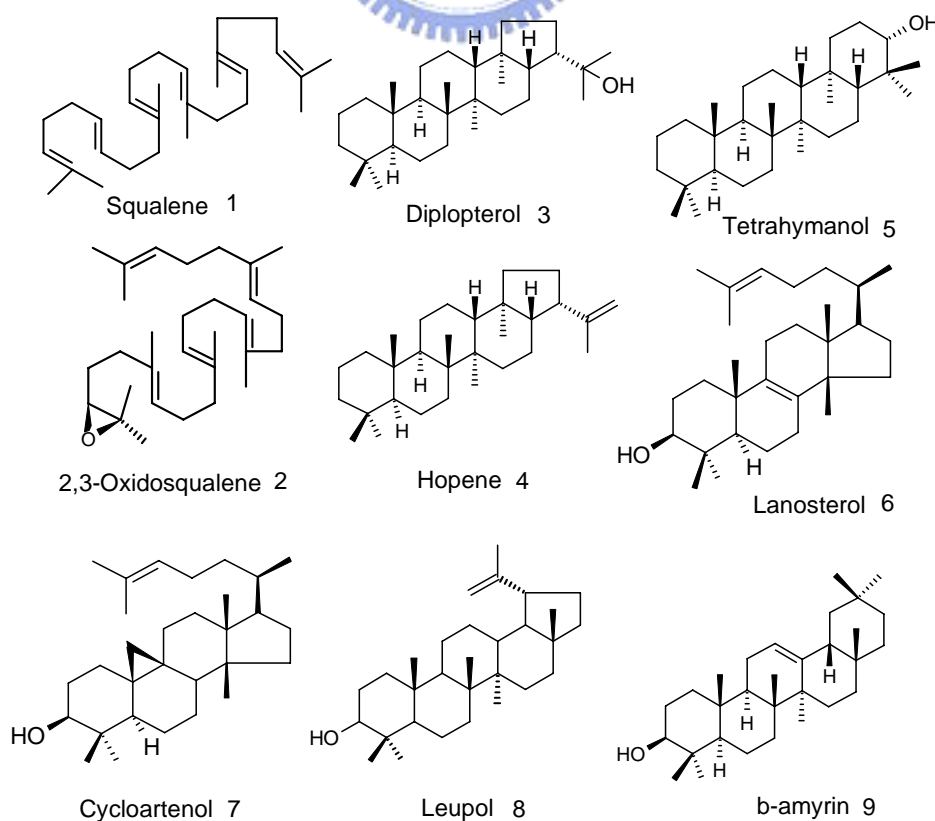


Figure 1-3. The sterol biosynthesis pathway in nature.

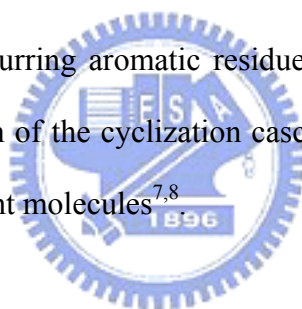
1.2 Triterpene cyclases

Terpenoids, which constitute the largest group of natural products, are the metabolites of the cyclic or acyclic hydrocarbons known as terpenes. Terpene synthases construct the carbocyclic skeletons either by eliminating the allylic pyrophosphate from prenyl pyrophosphate or by protonating an epoxide olefin. The resultant carbocations are under proton abstraction, water addition or another nucleophile attraction. A central reason for that terpene diversity is that terpene synthases are groups of plastic enzyme acquired novel catalytic properties via the rapidly mutational changing². Oxidosqualene cyclase constitute a family of enzymes that catalyze diverse and complex carbocationic cyclization/rearrangement reaction of squalene **1** or (3*S*)-2,3-oxidosqualene (OS) **2** into various triterpenes including diplopterol **3**, hopene **4**, tetrahymanol **5**, lanosterol **6**, cycloartenol **7**, leupol **8**, and β -amyrin **9**. These triterpenes in turn serve as the precursors of all hopanoids and sterols, including cholesterol, glucocorticoids, and hormones³.



1.3 Oxidosqualene-Lanosterol cyclase

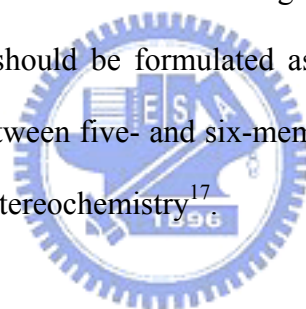
The oxidosqualene cyclases (OSCs), eukaryotic enzymes that convert oxidosqualene to polycyclic triterpenes, are remarkable for one-step cyclization/rearrangement reactions. Complexity, efficiency, and high stereoselectivity of cyclase catalyzed reaction make them prime examples for studying multiple function enzyme. Additionally, cyclases are also of high economical interest as target in the development of antifungal, hypocholesterolemic, and phytotoxic drugs. Various and high product specificity in cyclases is believed to be achieved through several factors: (1) by enforcing substrate to occupy prefolded conformations^{4,5}, (2) by progression of reaction via rigidly held, partially cyclized carbocationic intermediates^{4,6}, and (3) by stabilization of intermediate carbocationis via π -cation interactions of frequently occurring aromatic residues in the active site cavity, thus preventing the early formation of the cyclization cascade due to the deprotonation or nucleophilic addition of solvent molecules^{7,8}



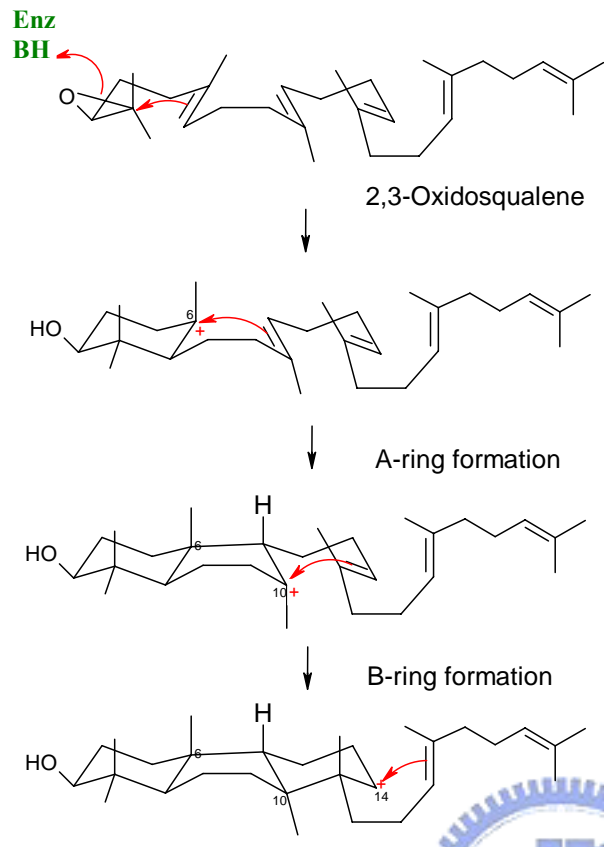
Mechanism of cyclization

Product specificity and diversity are species dependent and mainly controlled by the prefolded substrate conformation within the enzyme active site as well as the molecular interaction between carbocation intermediate and the functional group of amino acid residues. We now know that the formation of lanosterol and cycloartenol proceeds via the so-called “chair-boat-chair” conformation of substrate in the enzyme active site and that the cyclization is initiated by acid-catalyzed epoxide ring opening with participation of a neighboring acid residue^{4,6} (Scheme I). The cyclization was progressed via a series of 1,2-nucleophilic attack until a protosteryl C-20 cation formation. A series of 1,2-methyl and hydride group shifts coupled with the final deprotonation reaction were carried out to yield either lanosterol or cycloartenol

skeleton. Similarly, the cyclization of the same substrate to pentacyclic triterpenes such as leupol and β -amyrin appears to proceed via the corresponding “chair-chair-chair” conformation of the substrate. The tetracyclic dammarenyl C-20 cation is corresponding for the protosteryl cation in the pentacyclic triterpene pathways⁹. Indeed, monocyclic and bicyclic triterpenes, which are thought to be “trapped” partially cyclized intermediates, have been isolated from nature^{10,11}. During the enzymatic cyclization of oxidosqualene, the six-membered C-ring is formed via a thermodynamically unfavorable secondary (6.6.6-fused) tricyclic cation in an anti-Markovnikov addition¹². In contrast, non-enzymatic cyclization of oxidosqualene produces 6.6.5-fused tricyclic products, which are formed from a thermodynamically favored tertiary cation with a five membered C-ring¹³⁻¹⁶. van Tamelen proposed that such an intermediate cation should be formulated as a nonclassical species to best rationalize the partitioning between five- and six-membered rings and to maintain the proximity carbons as well as stereochemistry¹⁷.

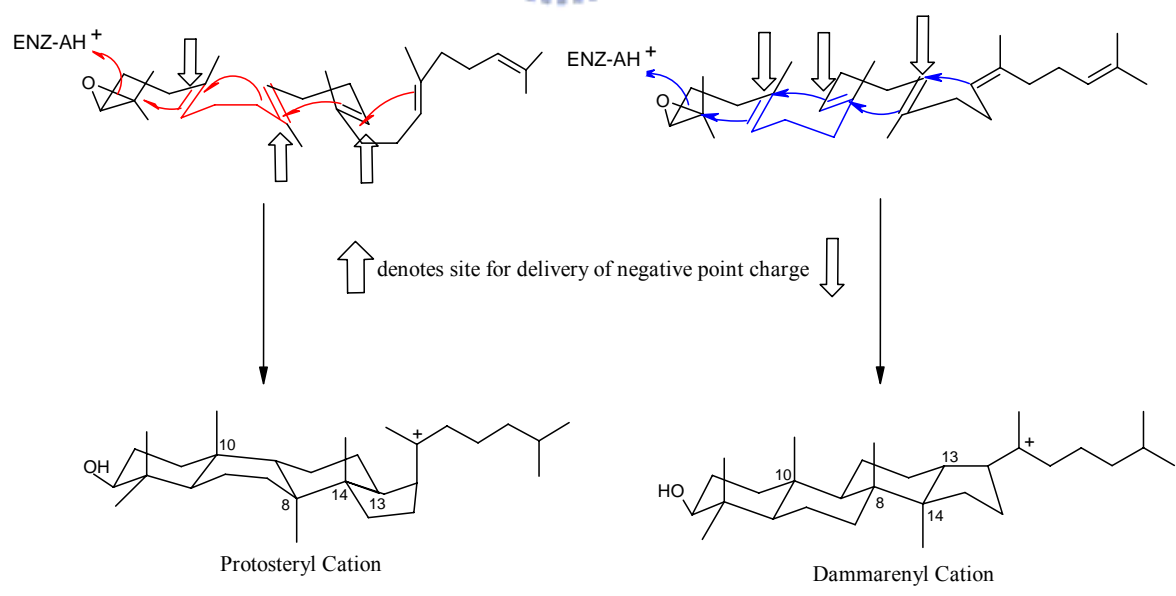


Corey and Virgil demonstrated that the D ring closure during lanosterol formation produces a protosterol cation with the 17β - oriented side chain by analogue of 2,3-oxidosqualene. In this case, the initially formed conformation of the protosteryl C-20 cation can lead to the natural C-20*R* configuration via a rotation of the C-17 to C-20 axis. Further, the β - orientation of the side chain at C-17 is thought to facilitate the control of configuration at C-20 in lanosterol formation, since the protosterol cation is generated for hydride migration and bond rotation^{6,18,19}.



Scheme I
Oxidosqualene cyclase catalyzes the cyclization of oxidosqualene to form lanosterol.

Scheme II



What is the catalytic mechanism of oxidosqualene cyclase and how does it to stabilize the high energetic carbocation intermediate during the cyclization/rearrangement cascades? In 1987, Johnson proposed a hypothetical mechanism for the action of oxidosqualene cyclase. The axial delivery of negative charges are involved by the enzyme so ion pairs formation could stabilize the progressing cationic center on the cyclizing substrate^{7,20} (Fig. 1-4). Johnson's theory provides a stereo-electronic aspect to understand the polycyclization mechanism. The negative point charge can also be used to explain the closure of the B-ring in a boat conformation, as well as the *anti*-Markovnikov C-ring closure (Scheme II). The delivery of a point charge to the α -face at *pro*-C8 could lower the activation energy of the B-ring boat conformation relative to the chair alternative^{13,21}. Another point charge proximal to the α -face at *pro*-C-13 but not to *pro*-C-14 could guide the course of reaction in the *anti*-Markovnikov manner. It has been further postulated that such charge delivery to the β -face at *pro*-C-10 might be important in enhancing the rate and efficiency of the overall cyclization process^{9,14,18,22}.

However, other steric forces such as hydrophobic interaction and cation- π interaction could shelter cation, and there is reason to believe that the aromatic amino acid residues at the active site might play a crucial role in the cyclization reaction. The aromatic hypothesis model was issued in 1992 by John Griffin. The central section described that the aromatic amino acids located at the active site cavity were highly conserved to provide the stabilizing force facing the cationic intermediate by π -cation interactions⁸ (see Fig. 1-5).

Fig. 1-4 : Johnson Model proposes that the high-energy carbocation intermediates were stabilized in the active site of the enzyme by the negative charge interactions of amino acid residues^{7,20}.

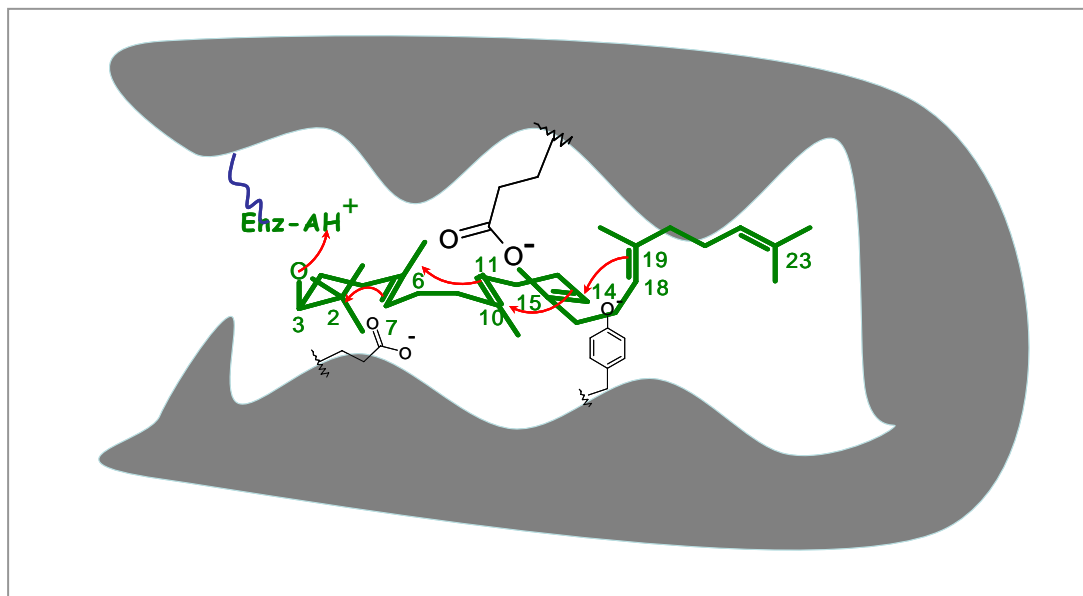
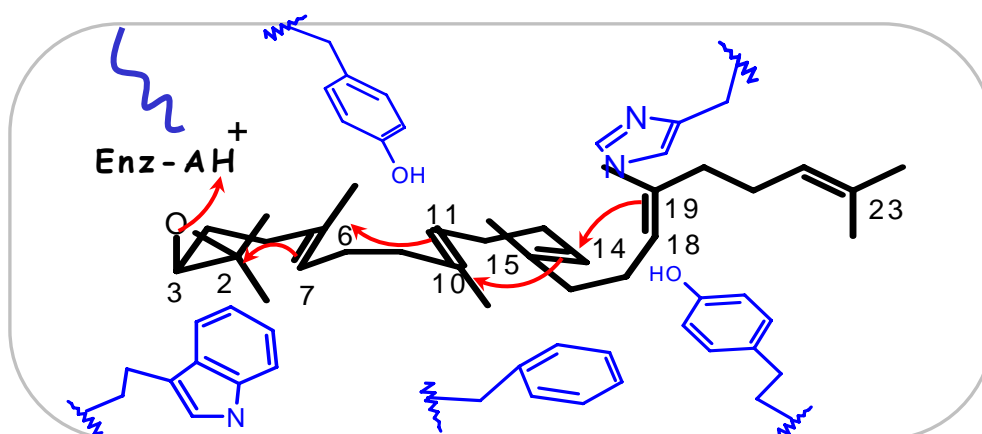


Fig. 1-5. Aromatic hypothesis model: the highly conserved aromatic acid residues in the active site cavity might stabilize the cationic intermediates during cyclization developing⁸.

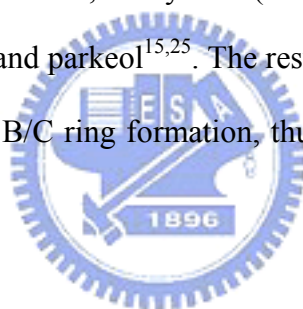


The Studies on Site-Directed Mutagenesis

With the long-term absence of a crystal structure for oxidosqualene cyclase highlighted the importance of mutagenesis studies to understand the mechanism of oxidosqualene cyclization. First, Corey predicted the putative active site of oxidosqualene cyclase in *Saccharomyces cerevisiae* by bioorganic data and determined the essential residues for catalytic activity¹⁸. Using site-directed mutagenesis, Corey successfully identified His146, His234, and Asp456 residues which were believed to be essential for catalytic activity^{6,18}. *S. cerevisiae* ERG7 derivatives with these residues mutated to Ala residue could not complement the yeast lanosterol synthase knockout strain indicated the importance of these residues. They suggested a model where protonated His146 enhances the acidity of the proton donor and Asp456 which initiates the cyclization reaction. His234 is implicated in protosteryl cation stabilization. His234 can be replaced by phenylalanine without loss of activity, but not by alanine, lysine, or arginine. This is consistent with its proposed role for cation stabilization via π -cation interaction¹⁸.

In early work to understand how oxidosqualene-lanosterol cyclase effects catalysis, Corey used 2,3-oxidosqualene analogues to demonstrate that His146, His234, and Asp456 were shown to be catalytically essential. They suggested the initial activation and substrate conformation impacted the rate of cyclization. For example, the protonated His146 could enhance Asp456, corresponding to Asp376 residue in squalene-hopene cyclase, to increase the cyclization reaction rate by forming nucleophilic group to attack the epoxide ring of (3*S*)-2,3-oxidosqualene¹⁹. As previously mentioned, oxidosqualene is believed to be profolded via the chair-boat-chair conformation by enzyme active site. B-ring formation is concerted and C-ring formation is a 5-exo Markovnikov process. In least five years, the

site-saturated/directed mutagenesis experiments on the putative active site residues with *S. cerevisiae* ERG7, including Trp232, His234 and Tyr510 were carried out^{15,16,23,24}. This ideal approach would be performed to investigate the structure-reactivity relationships between amino acid residues and cationic intermediates. According to His 234 saturated mutants, the isolation of (13 α Z)-isomalabarica-14(26), 17Z, 21-trien-3 β -ol and protosteryl-20,24-dien-3 β -ol provides long-sought support for the hypothesis that formation of lanosterol from oxidosqualene in ERG7-catalyzed cyclization/rearrangement reaction proceeds via the Markovikov C-B 6-6-5 tricyclic cation²⁴. Additionally, the mutations of Tyr510 residue of the oxidosqualene-lanosterol cyclase from *Saccharomyces cerevisiae* produced monocyclic achilleol A, tricyclic (13 α Z)-isomalabarica-14(26), 17Z, 21-trien-3 β -ol, and lanosterol and parkeol^{15,25}. The results suggested that the Tyr510 is positioned proximal to A and B/C ring formation, thus affecting ring cyclization and final deprotonation²⁶.



Recently, Thoma *et al.* have succeeded in determining the structure of human OSC complex with the product lanosterol, providing an important additional snapshot of the triterpene polycyclization cascades²⁶. At the “top” of the cavity from human OSC crystal structure, the side chain of Asp455 hydrogen bonds with the lanosterol hydroxyl group, consistent with the proposed role of Asp455 as the general acid that donated a proton to the epoxide oxygen of the substrate to initiate the cyclization cascades. The side chain of Asp-455 also accepts hydrogen bonds from Cys-456 and Cys533, which might enhance the acidity of Asp455. Thoma and colleagues suggested that reprotonation of Asp455 could be achieved by bulk solvent through a hydrogen bonded solvent network with Glu459 in the polar channel leading to Asp455²⁷ (Fig. 1-6).

The complex structure of OSC with lanosterol suggests how the energetically unfavorable boat conformation of the B-ring is induced. Thoma *et al.* suggested that Tyr98 might preferentially stabilize the substrate in the unfavorable boat conformation required for lanosterol B-ring formation (Fig. 1-7). The unstable secondary carbocation at C-14 produced during the C-ring anti-Markovnikov manner cyclization could be stabilized via the side chain of His232 and Phe696 by the appropriate orientation²⁶.

The closure of the D-ring yields the protosteryl C-20 cation, which is subsequently converted into lanosterol by 1, 2-hydride and methyl group migration reactions. A hydrogen bond with Tyr503 appears to be sufficient to prevent His232 from adopting a conformation that reached with C-14 carbocation²⁸. Thoma and colleagues suggested that His232 and Tyr503 residues are essential and strictly conserved among oxidosqualene cyclase (Fig.1-8). Both of them are possible candidates for the role of base that accept the C-9 proton to terminate the cyclization/rearrangement reactions cascades²⁶. Now, a three-dimensional crystal structure of human oxidosqualene cyclase is available, the active site residues could be probed to clarify the structure-function relationships for this triterpene cyclase²⁶.

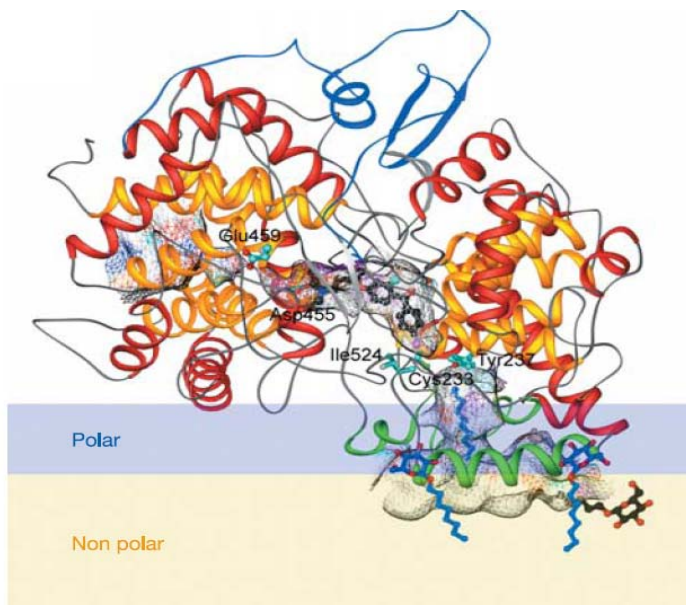


Fig. 1-6 Panel shows a model of human oxidosqualene cyclase associated with a membrane leaflet. Internal surfaces are colored as follows: blue, positive; red, negative; cyan, hydrogen bond donor; magenta, other polar²⁶.

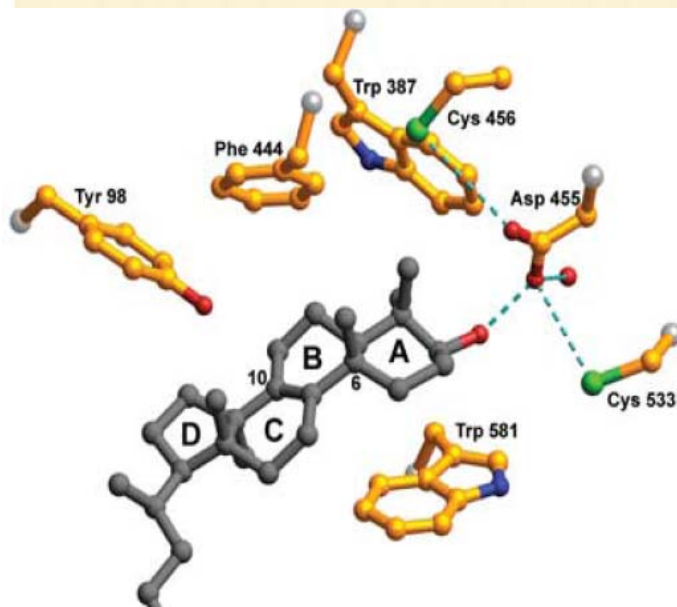


Fig. 1-7 This panel shows the hydroxyl group of lanosterol donates a hydrogen bond to active site general acid, Asp455. The aromatic side chains of Trp387, Phe444, and Trp581 are suitably oriented to stabilize carbocation intermediates formed at C6 and C10 during the cyclization sequence through π -cation interactions²⁶.

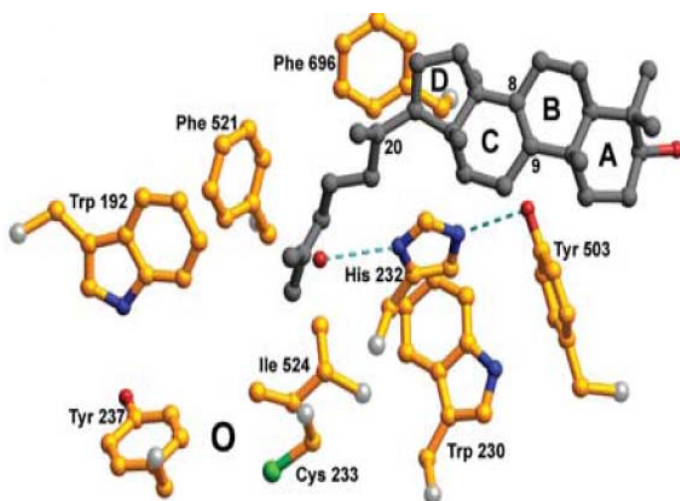
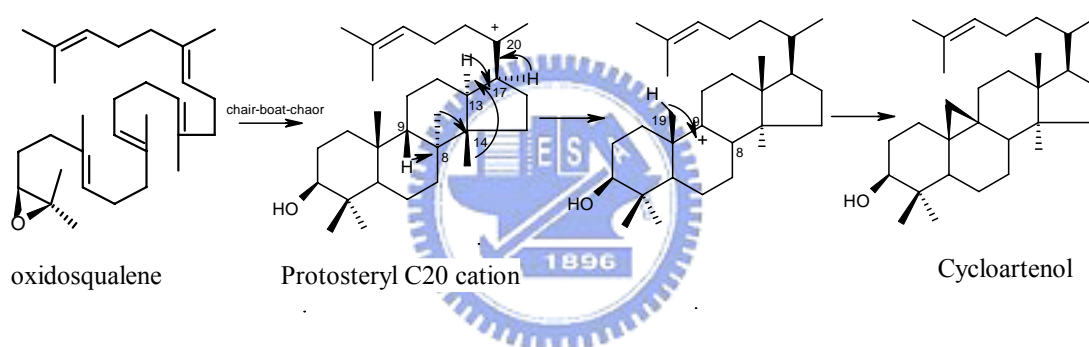


Fig. 1-8 The aromatic side chains of Phe696 and His232 are suitably oriented to stabilize the penultimate carbocation intermediates at C20 through cation- π interactions. Either His232 or Tyr503 is oriented to accept the C9 proton in the final elimination step yield lanosterol²⁶.

1.4 Cycloartenol Cyclase

Mechanism of Cyclization

In higher plants, oxidosqualene is the biosynthetic precursor common to both steroids and triterpenoids. Oxidosqualene is cyclized to cycloartenol, which corresponds to lanosterol in animals and fungi during phytosterol biosynthesis²⁹. The postulated mechanism of conversion of oxidosqualene into cycloartenol is the same as that for lanosterol cyclization, except for the final 9 β ,19-cyclopropane ring closure instead of C-9 proton elimination. The final migration of hydrogen of the C-19 methyl group would be *cis* to the preceding C-9 hydrogen migration³⁰.



Both of cycloartenol synthase and oxidosqualene cyclase contain ~700 amino acids and are 30-46% identical at the amino acid level, according to the information of sequence alignment. Some of ~400 residues that differed between cycloartenol synthase and oxidosqualene-lanosterol cyclase might impact the catalytic distinction between these two enzymes. Identifying and characterizing the catalytically important residues would clarify the relationships of products diversity between cycloartenol synthase and oxidosqualene-lanosterol cyclase.


The Studies on Site-Directed Mutagenesis

Recently, an alternative to random mutagenesis coupled with genetic selection strategy was used to identify catalytically important residues involved in these two cyclases. In the sequence alignment result, Tyr410, Ile481, and His477 were strictly conserved in cycloartenol synthases, but a different residue replaced at the corresponding position in oxidosqualene-lanosterol cyclase were observed³¹. (Figure 1-9, 1-10, and 1-11). For example, the catalytically important *AthCAS1* Ile481 is corresponding to the strictly conserved Val454 in the *Saccharomyces cerevisiae* oxidosqualene cyclase. An Ile481Val mutation introduced a subtle steric change by substituting an isopropyl side chain in place of sec-butyl side chain. Conversion of oxidosqualene to 25% lanosterol means that Ile481 is not catalytically essential, but might provide steric bulk to align the substrate and active site base for the cycloartenol formation. The side chain substitutions of Val454 by alanine and glycine produce primarily lanosterol, but also minor amounts of achilleol A. Val454 apparently participates in proper substrate folding and mutation of this residue to a smaller residue might allow the substrate or an active-site base to adopt a fixable conformation that terminates the reaction after monocyclic formation³². Similarly, the substitutions of Tyr410 and His477 would convert particular oxidosqualene to lanosterol and/or parkeol products³³.

According to these experiment dates, Matsuda and colleagues suggested that Tyr410 mutants apparently produced product derived from C-9 cation hence the Tyr410 might facilitate the C-9 to C-8 hydride shift during oxidosqualene cyclization. The Tyr410Thr and Ile481Val mutations might block the hydride shift from C-9 to C-8 and this alternatively precludes the opportunity for His477 mutations to promote the formation of parkeol³⁴. The product profiles ratio of these *AthCAS1* mutants were

showed in Table-1.

Interestingly, a pervious mutagenic study of *AthCAS1* showed that a double mutant, His477Asn Ile481Val, produced 99% lanosterol and 1% parkeol. The corresponding residues of OSC7 (lanosterol synthase in *Archaeplastida Lotus*) are Asn478 and Val482³⁵. Interestingly, replacement of asparagine with histidine and valine with isoleucine produced the major and minor compounds, parkeol and cycloartenol. These findings strongly suggested that lanosterol synthase emerged from the ancestral cycloartenol synthase in different lineages by convergent evolution, which is consistent with some previous hypotheses^{6,36}. Although no direct findings contradict that plant lanosterol might act as an alternative intermediate for the sterol or a precursor of other significant metabolites, identification of lanosterol metabolizing enzymes is the key to understanding the physiological roles of plant sterol³⁷.



<i>AthCAS1</i>	G	M	K	M	Q	G	Y	N	G	S	Q	L	W	416
<i>PsaCAS1</i>	G	M	K	M	Q	G	Y	N	G	S	Q	L	W	416
<i>PglCAS1</i>	G	M	K	M	Q	G	Y	N	G	S	Q	L	W	416
<i>GglCAS1</i>	G	M	K	M	Q	G	Y	N	G	S	Q	L	W	416
<i>LcyCAS1</i>	G	M	K	M	Q	G	Y	N	G	S	Q	L	W	424
<i>AsaCAS1</i>	G	M	K	M	Q	G	Y	N	G	S	Q	L	W	417
<i>DdlCAS1</i>	G	M	K	M	Q	G	Y	N	G	S	Q	L	W	369
<i>SceERG7</i>	G	M	T	I	M	G	T	N	G	V	Q	T	W	390
<i>CaERG7</i>	G	M	T	V	M	G	T	N	G	V	Q	V	W	384
<i>CcaERG7</i>	G	M	L	V	N	G	T	N	G	V	Q	C	W	412
<i>SpoERG7</i>	G	M	L	M	R	G	T	N	G	L	Q	V	W	385
<i>RnoERG7</i>	G	M	K	M	Q	G	T	N	G	S	Q	T	W	388
<i>HsaERG7</i>	G	M	K	M	Q	G	T	N	G	S	Q	I	W	387

Fig. 1-9 Tyrosine is strictly conserved in the cycloartenol synthases (CAS1), but threonine is conserved at the corresponding position in lanosterol synthases (ERG7).

<i>AthCAS1</i>	A	D	H	G	W	P	I	S	D	C	T	A	E	487
<i>PsaCAS1</i>	A	D	H	G	W	P	I	S	D	C	T	A	E	487
<i>PgiCAS1</i>	A	D	H	G	W	P	I	S	D	C	T	A	E	487
<i>GglCAS1</i>	A	D	H	G	W	P	I	S	D	C	T	A	E	487
<i>LcyCAS1</i>	A	D	H	G	W	P	I	S	D	C	T	A	E	495
<i>AsaCAS1</i>	A	D	H	G	W	P	I	S	D	C	T	A	E	488
<i>DdiCAS1</i>	V	D	H	G	W	P	I	S	D	C	T	A	E	439
<i>TbrERG7</i>	R	P	Q	A	W	Q	V	S	D	C	T	A	E	625
<i>TcrERG7</i>	A	S	Q	S	W	Q	V	S	D	C	T	A	E	616
<i>SceERG7</i>	K	T	Q	G	Y	T	V	A	D	C	T	A	E	460
<i>CalERG7</i>	K	E	Q	G	Y	T	V	S	D	C	T	A	E	454
<i>CcaERG7</i>	K	D	Q	G	Y	A	V	S	D	C	T	S	E	484
<i>SpoERG7</i>	I	T	Q	G	Y	T	V	S	D	T	T	S	E	455
<i>RnoERG7</i>	L	D	C	G	W	I	V	A	D	C	T	A	E	460
<i>HsaERG7</i>	L	D	C	G	W	I	V	S	D	C	T	A	E	459

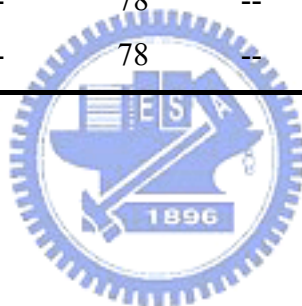
Fig. 1-10 Isoleucine is strictly conserved in the cycloartenol synthases (CAS1), but valine is conserved at the corresponding position in lanosterol synthases (ERG7).

<i>AthCAS1</i>	P	F	S	T	A	D	H	G	W	P	I	S	D	483
<i>PsaCAS1</i>	P	F	S	T	A	D	H	G	W	P	I	S	D	483
<i>PgiCAS1</i>	P	F	S	T	A	D	H	G	W	P	I	S	D	483
<i>GglCAS1</i>	P	F	S	T	A	D	H	G	W	P	I	S	D	483
<i>LcyCAS1</i>	P	F	S	T	A	D	H	G	W	P	I	S	D	491
<i>AsaCAS1</i>	P	F	S	T	A	D	H	G	W	P	I	S	D	484
<i>DdiCAS1</i>	P	F	S	T	V	D	H	G	W	P	I	S	D	435
<i>TbrERG7</i>	N	F	S	T	R	P	Q	A	W	Q	V	S	D	621
<i>TcrERG7</i>	N	F	S	T	A	S	Q	S	W	Q	V	S	D	612
<i>SceERG7</i>	G	F	S	T	K	T	Q	G	Y	T	V	A	D	456
<i>CalERG7</i>	P	F	S	T	K	E	Q	G	Y	T	V	S	D	450
<i>CcaERG7</i>	P	F	S	N	K	D	Q	G	Y	A	V	S	D	480
<i>SpoERG7</i>	P	F	S	N	I	T	Q	G	Y	T	V	S	D	451
<i>RnoERG7</i>	P	F	S	T	L	D	C	G	W	I	V	A	D	456
<i>HsaERG7</i>	S	F	S	T	L	D	C	G	W	I	V	S	D	455

Fig. 1-11 Histidine is strictly conserved in the cycloartenol synthases (CAS1), but glutamine is conserved at the corresponding position in lanosterol synthases (ERG7).

Table 1 The product ratios of *AthCAS1* Tyr410, Ile481, and His477 mutants.

<i>AthCAS1</i> mutants	Cycloartenol	Lanosterol	Parkeol	⁹ β - Δ 7-Lanosterol	Achilleol A	Camelliol C
CAS ^{I481}	99	--	1	--	--	--
CAS ^{I481L}	83	1	16	--	--	--
CAS ^{I481V}	55	24	21	--	--	--
CAS ^{I481A}	12	54	15	--	13	6
CAS ^{I481G}	17	23	4	--	44	12
CAS ^{Y410T}	--	65	2	33	--	--
CAS ^{Y410C}	--	75	--	24	1	--
CAS ^{H477N}	--	88	12	--	--	--
CAS ^{H477Q}	--	22	73	5	--	--
CAS ^{I481V/ Y410T}	--	78	< 1	22	--	--
CAS ^{I481V/ H477N/ Y410T}	--	78	--	22	--	--
CAS ^{I481V/ H477Q/ Y410T}	--	78	--	22	--	--



1.5 Squalene-Hopene Cyclase

Squalene-hopene cyclase catalyzes the cyclization of squalene to form the pentacyclic hydrocarbon hopene (Fig. 1-12). On the basis of the crystal structure of squalene-hopene cyclase complexed 2-azasqualene (Fig. 1-13), the cyclization of squalene, prefolded in all prechair conformation, is initiated by a proton attack on a terminal double bond and followed by addition of water at the resulting gammaceranyl C-21 cationic center without carbon skeleton rearrangement. Hopene is a biosynthetic precursor of the bacterial hopanoids, which modulate membrane fluidity. The X-ray crystal structure of squalene-hopene cyclase from *Alicyclobacillus acidocaldarius* revealed a dimeric enzyme: each monomer contains two domains, and each domain adopts double α -barrel fold. Two domains assemble to enclose a central hydrophobic active site cavity^{22,38} (Fig. 1-14).

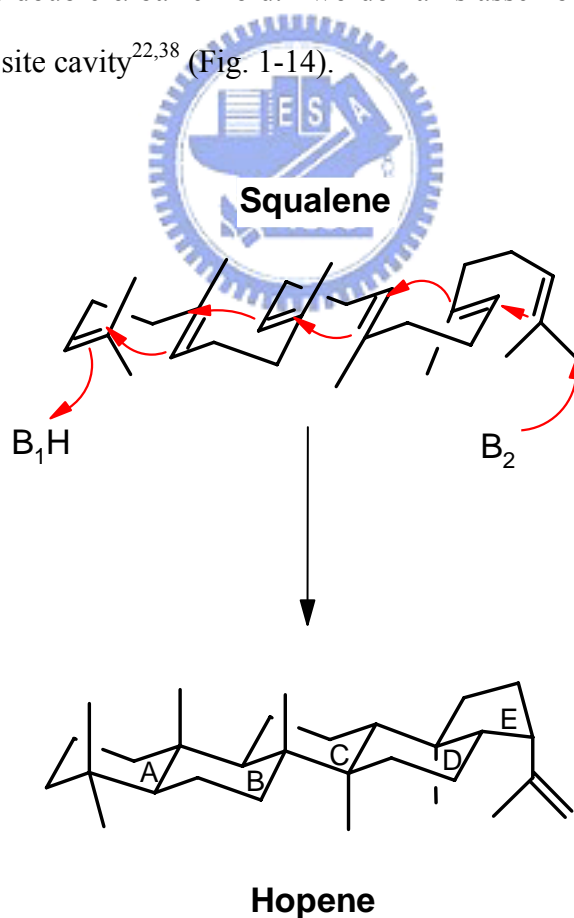


Fig. 1-12 Squalene-hopene cyclase reaction. Various data indicate that general acid $B_1:H$ is Asp-376, which protonates squalene at C3 and triggers the cyclization cascade. The $B_2:H$ is general acid base for the final deprotonation step at C29²².

Fig. 1-13. Electron density map showing the precise binding conformation of the inhibitor 2-azasqualene in the active site of squalene-hopene cyclase.

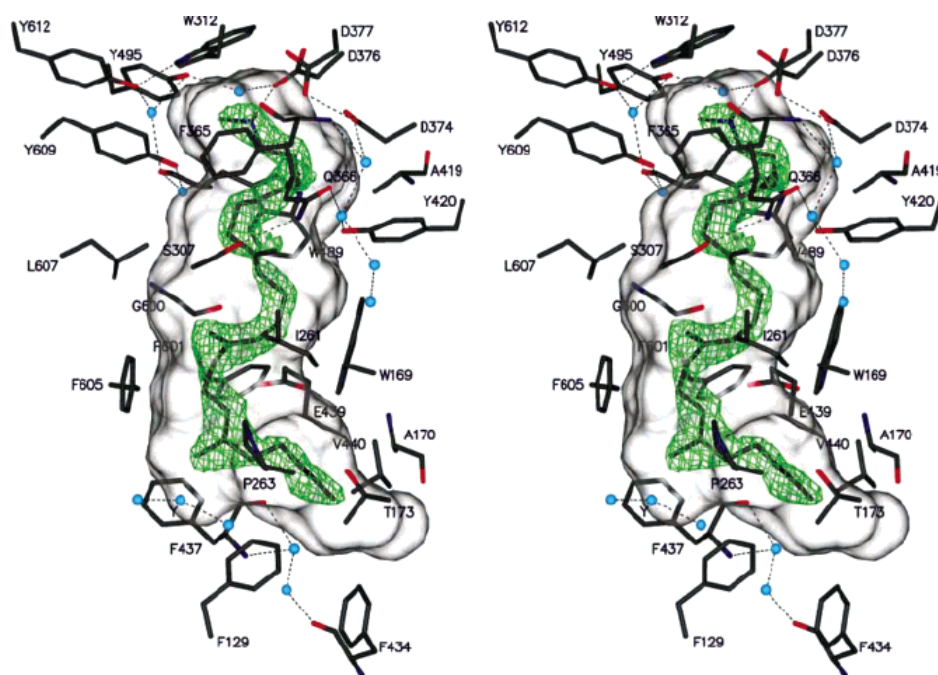
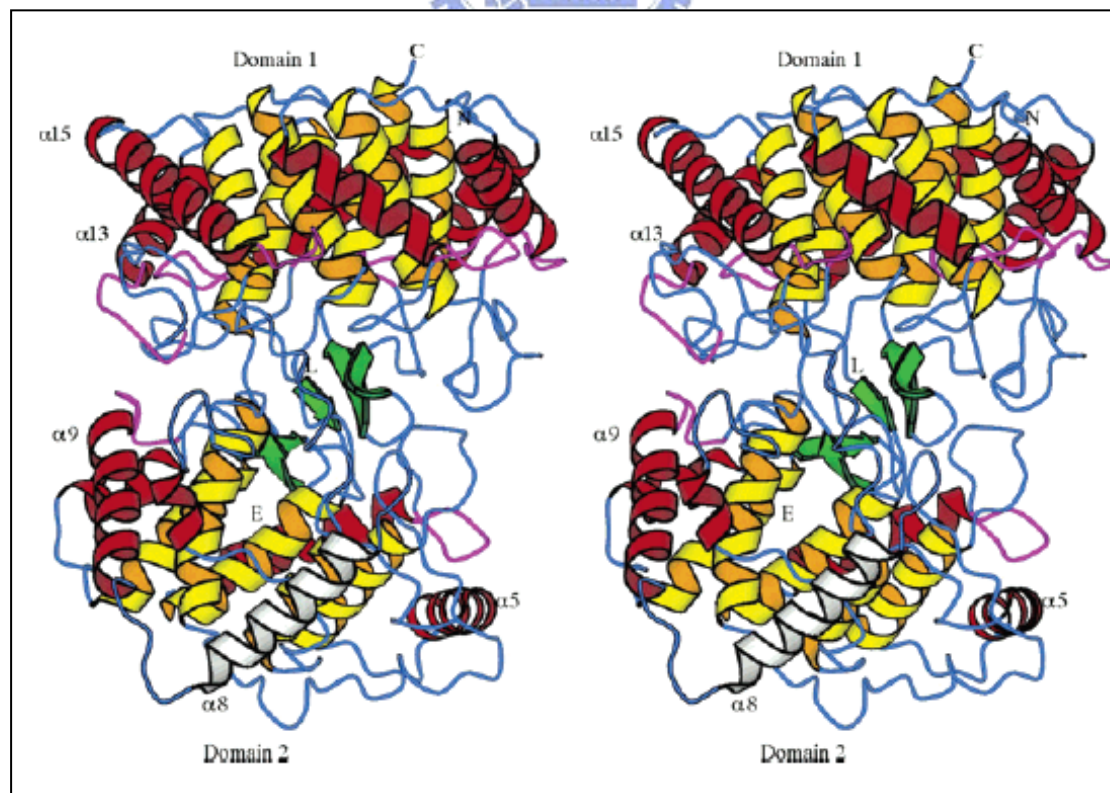


Fig. 1-14. Structure of the squalene-hopene cyclase monomer.



The Studies on Site-Directed Mutagenesis

Together with the three-dimensional structure and enzyme-labeling experiments, recent mutagenesis results allow for the first time detailed discussion of specific π -cation interactions in the triterpene cyclases. For example, mutation of Tyr420 (corresponding to Tyr510 in yeast oxidosqualene cyclase) to alanine leads to the production of bicyclic triterpenes **10** and **11** and minor amounts of tricyclic compound **12**³⁹. The result shows that the truncated products might arise from premature quenching of C10 B-ring cation, which might be stabilized by its proximity to Tyr420. In another case, Phe601 residue, which is highly conserved in triterpene cyclases is believed to stabilize the C18 carbocation that results from 5-*exo* Markovnikov D-ring closure⁴⁰. Loss of this stabilization might lead to truncate the polycyclization, resulting from premature termination of the carbocation intermediates¹⁰. Replacement of Phe601 (corresponding to Phe699 in yeast oxidosqualene cyclase) with alanine results in an increasing production of **13**, accompanied by lower yield of two tricyclic compounds **14** and **15**⁴¹. These findings suggested that residue Phe601 might stabilize C19 cation intermediate by π -cation interactions and might interact with a 6-6-5 Markovnikov cation intermediate^{10,42}.

Mutation of Trp169 in the center of the active-site cavity to the less electron-rich residues Phe and His resulted in increasing amounts of 6-6-6-5 fused ring compound **13** (see Fig. 1-15). This finding suggested that residue Trp169 might stabilize C19 cation intermediate by π -cation interactions⁴³. Surprisingly, the mutations of Trp489, which is adjacent to Tyr420 in the upper part of the active site, resulted in significantly increased production of **13**. These results might be explained that the aromatic residues, such as Trp169, Tyr420, and Trp489 can stabilize the position of C19 in cyclization reactions via π -cation interactions.

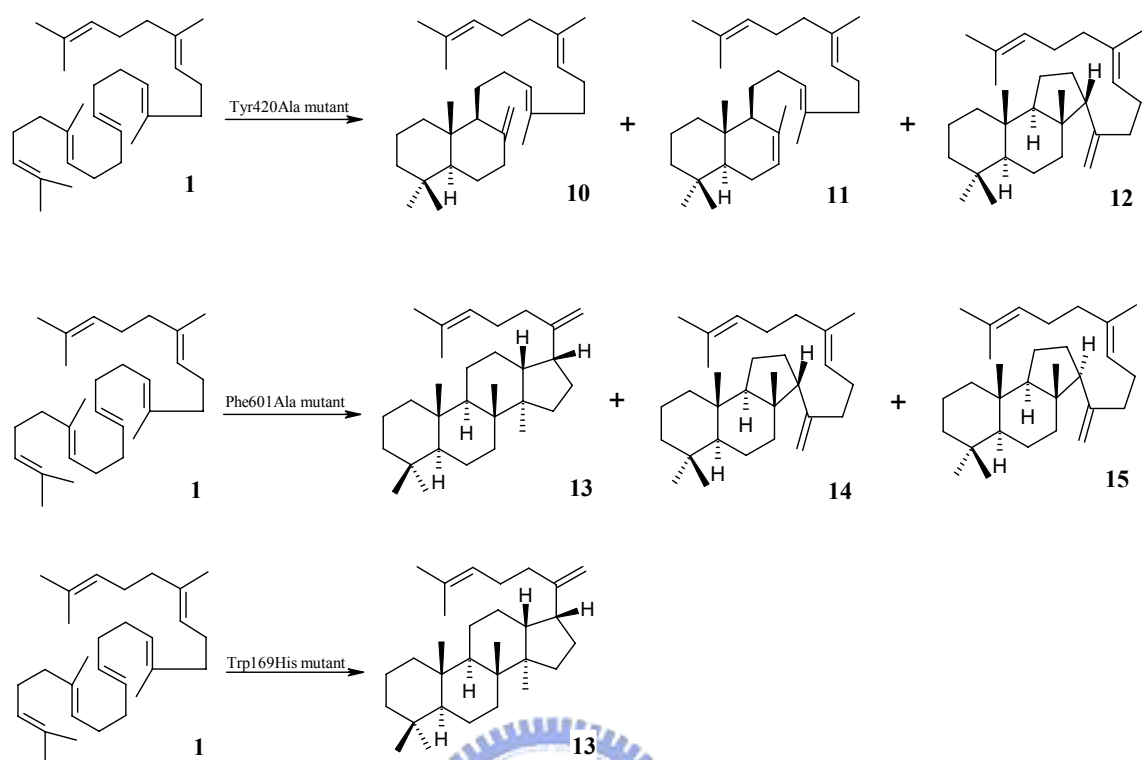


Fig. 1-15. Partially cyclized products resulting from the incubation of squalene with squalene-hopene cyclase bearing mutations at putative cation stabilizing residues.

1.6 Sequence Alignment and Homology Modeling

In order to clarify the functional residues in the active site cavity of oxidosqualene cyclases for developing antifungi and hypocholesterolemic drugs, we use the program of ClusterW for sequence alignment to predict the active site cavity of oxidosqualene cyclase. The characterized enzymes are as follows: *H. sapoens* OSC: P48449, *S. cerevisiae* OSC: P38604, cyclartenol synthase from *A. thaliana*: P38605, *A. acidocaldarius* SHC: P33247. All of them were obtained from the Protein Data Bank (PDB). The result of sequence alignment was shown in below (Fig.1-16).



```

Hs_ OSC      MTEGTCLRRRGGPYKTEPATDLGR--WRLNCERGR-----QTWTYLQDERAGREQTG 50
At_ CAS      -MWLKI AEGGSPWLRTTNNHVGRQFWEFDPNLGTPEDLAAVEEARKSFSDNRVQKHS 59
Sc_ OSC      -MTEFYSDTIG---LPKTDPRLWR---LRTDELGR-----ESWEYLTPQQAANDPPS 45
Aa_ SHC      -----MAEQLVEAP-- 9

Hs_ OSC      LEAYALGLDTKNYFKDLP-----KAHTAFEGALN-GMTFVYVGLQAED-GHWTGDY 98
At_ CAS      DLLMRLQFSRENLI SPVLPQVKIEDTDDVTEEMVETTLKRGLDFYSTIQAHD-GHWPGDY 118
Sc_ OSC      TFTQWLLQDPK-FPQHPERNK----HSPDFSAFDACHN-GASFFKLLQEPDSGIFPCQY 99
Aa_ SHC      -----AYARTLDRAVEYLLSCQKDE-GYWWGGL 36

Hs_ OSC      GGPLFLLPGLLI TCHVARIP--LPAGYREEIVRYLRSVQL-PDGGWGLHIEDKSTVFGT 154
At_ CAS      GGPMFLLPGLI I TLSITGALNTVLSEQHKQEMRRYLYNHQN-EDGGWGLHIEGPMSTMFGS 177
Sc_ OSC      KGPMFMTIGYVAVNYIAGIE---IPEHERIELIRYIVNTAHPVDGGWGLHSVDKSTVFGT 156
Aa_ SHC      LSNVTMEAEYVLLCHILDRVD---RDRMEKIRRYLLHEQR-EDGTWALYPGGPPDLDTT 91

Hs_ OSC      ALNYVSLRILGVGPDPPD--LVRARNILHKKGGAVAI PSWGKFWLAVLVNYSWEGLNRLF 212
At_ CAS      VLNYVTLRLLGEGPNDGDGMMEKGRDWILNHGGATNITSWGKMWLSVLGAFEWSGNNPLP 237
Sc_ OSC      VLNYVILRLLGLPKDHPV--CAKARSTLLRLGGAIGSPHWGKI WLSALNLYKWEGVNPAP 214
Aa_ SHC      IEAYVALKYIGMSRDEEP--MQKALRFIQSQGGIESSRVFTRMWLALVGEYVPEKVPMPV 149

```


Hs_OSC PEMWLFDPWAPAH PSTLWCHCRQVYLPMSYCYAVRLSAAEDPLVQSLRQELYVEDFASID 272
 At_CAS PEI WLLPYFLPIHPGRMWCHCRMVYLPMSYLYGKRFVGPITSTVLSLRKELFTVPYHEVN 297
 Sc_OSC PETWLLPYSLPMHPGRWVCHITRGVYIPVSYLSLVKFSCPMTPLLEELRNEIYTKPFDKIN 274
 Aa_SHC PEIMFLGKRMP LNIYEFGSWARATVVALSIVMSRQPVFPLPERARVP--ELYETDVPPRR 207

Hs_OSC WLAQRNNVAPDELYTPHSWLLRVVYALLN-----LYEHHHS-AHLRQRAVQKLYEHI VAD 326
 At_CAS WNEARNLCAKEDLYYPHPLVQDILWASLHKI VEPVLMRWPG-ANLREKAI RTAIEHIHYE 356
 Sc_OSC FSKNRNTVCGVDLYYPHSTTLNIANS LVV-----FYEKYLRNRFIYSLSKKKVYDLIKTE 329
 Aa_SHC RGAKGG-----GGWIFDALDRALHG-----YQKLSVHPFRRAAEIRALDWLLERQ 252

Hs_OSC DRFTKSI SIGPI SKTINMLVRWYVDGPASTAFQEHVSRIPDYLMGLDGMKMQGTNGSQI 386
 At_CAS DENTRYICIGPVNKVLNMLCCWVED-PNSEAFKLHLPR IHDFLWLAEDGMKMQGYNGSQL 415
 Sc_OSC LQNTDSL CIAPVNQAFCALVTLIEEGVDSEAFQRLQYRFKDALFHGPGQMTIMGTNGVQT 389
 Aa_SHC AGDGSWGGIQPP-WFYALIALKILDMTQH PAFIKGWEGL ELYGV ELDYGGW MFQASISPV 311

Hs_OSC WDTAFAIQALLEAGGHRPEFSSCLQKAHEFLRLSQVPDNP -DYQKYRQMRKGGFSFS 445
 At_CAS WDTGFAIQAILATN--LVEEYGPVLEKAHSFVKNSQVLEDCPGDLNYWYRHSKGAWPFS 473
 Sc_OSC WDCAFAIQYFFVAGLAERPEFYNTI VSAYKFLCHAQFDTECV---PGSYDRKKGAWGFS 446
 Aa_SHC WDTGLAVLALRAAG--LPADHDRLVKAGEWLLDRQIT--VPGDWAVKRP NLKPGGFAFQ 366

Hs_OSC TLDCGWIVSDCTAEALKAVLLLQEKCP-HVT-EHIPRERLCDAVAVLLNMRNPD----GG 499
 At_CAS TADHGWPISDCTAEGLKAALLLSKVPK-AIVGEPIDAKRLEYAVNVIISLQAD----GG 528
 Sc_OSC TKTQGYTVADCTAEAIKAIIMVKNSPVFSEVHHMISSE RLFEGIDVLLNLQNI GSFEYGS 506
 Aa_SHC FDNVYYPDVDDTA VVVWALN TLR-----LPDERRRRDAMTKGFRWIVGMQSSN----GG 416

Hs_OSC FATYETKRGHLELLNPSEVFGDIMIDYTYVECTSAVMQALKYFHKRFPEHRAAEI RET 559
 At_CAS LATYELTRSYPWLELINPAETFGDIVIDYTYVECTSAAIQALISFRKLYPGHRKKEVDEC 588
 Sc_OSC FATYEKIKAPLAMETLNPAEVFGNIMVEYTYVECTDSSVLGLTYFHKYF-DYRKEEIRTR 565
 Aa_SHC WGAYDNDNTSDLPNHIPFCD-FG-EVTDPPSEDTVTAHVLECFG-----SFGYDDAWKV 467

Hs_OSC	LTQGLEFCRRQQRADGSWEGSWGVCFTYGTWFGLEAFACMGQTYRDGTACAEVSRACDFL	619
At_CAS	IEKAVKFIESIQAADGSWYGSWAVCVFTYGTWFGVKGLVAVGKTLKN---SPHVAKACEFL	645
Sc_OSC	IRIAIEFIKKSQQLPDGSWYGSWVICFTYAGMFALEALHTVGETYEN---SSTVRKGCDFL	622
Aa_SHC	IRRAVEYLKREQKPDGSWFGRWGVNLYGTGAVVSALKAVGIDTRE---PYIQKALDWV	523
Hs_OSC	LSRQMDGGWGEDFESCEERRY--LQSAQSQIHNTCWAMMGLMAVRHPDIEAQ--ERGVR	675
At_CAS	LSKQQPSGGWGESYLSQCDKVYSNLDGNRSHVNTAWAMLALIGAGQAEVDRKPLHRAAR	705
Sc_OSC	VSKQMKDGGWGESMKSSSELHSY--VDSEKSLVVQTAWALIALLFAEYPNKEVI--DRGID	678
Aa_SHC	EQHQNPDGGWGEDCRSYEDPAY--AGKGASTPSQTAWALMALIAGGRAESEEAR--RGVQ	579
Hs_OSC	CLLEKQLPNGDWPQENIAG-VENKSCAISYTSYRNIFPIWALGRFSQLYPERALAGHP	732
At_CAS	YLINAQMENGDFPQQEIMG-VENRNCMITYAAYRNIFPIWALGEYRCQVLLQQGE---	759
Sc_OSC	LLKNRQEESGEWKFESVEG-VENHSCAI EYPSYRFLFPIKALGMYSRAYETHL----	731
Aa_SHC	YLVETQRPDGGWDEPYTGTGEPGDFYLG YTM YRHVFP TLALGRYKQAIERR-----	631

Fig. 1-16. Sequence alignment of *Homo sapiens* (Hs) OSC, *Arabidopsis thaliana* (At) CAS, *Saccharomyces cerevisiae* (Sc) OSC, and *Alicyclobacillus acidocaldarius* (Aa) SHC. The markers are highly conserved residues in active site cavity of oxidosqualene cyclase. Black markers mean His234, Tyr510 and Phe699 residues in *S.cerevisiae* ERG7, respectively.

In these cyclases, the aromatic acid residues such as phenylalanine, tyrosine and tryptophane were highly conserved in the active site cavity of cyclases. It was suggested that the electron-rich residues could stabilize the cationic intermediates during the cyclization/rearrangement cascades. We previously predicted the putative active site in *S. cerevisiae* ERG7 and *A. thaliana* CAS1 via the crystal structure of squalene-hopene cyclase complexed with 2-azasqualene inhibitor^{22,26,27} (see Table 2). We also performed the alanine-screen experiments on these putative active site residues in *S. cerevisiae* ERG7. The results indicated the importance and the plasticity of amino acid residues in the catalytic mechanism of oxidosqualene cyclase.

CAS	OSC	SHC	CAS	OSC	SHC
Y118	Y99	L36	W416	W390	W312
F123	F104	T41	W470	W443	F263
L124	M105	M42	F472	F445	F365
P126	I107	A44	A475	K448	D368
G127	G108	E45	I481	V454	D374
H167	H146	Y81	D483	D456	D376
L179	L158	E93	C484	C457	D377
T215	P192	R127	Y532	Y510	Y420
W217	W194	F129	E548	E526	C435
W221	W198	W133	F550	F528	F437
M254	W231	F166	I553	I531	H431
W255	W232	G167	V554	M532	I432
H257	H234	W169	E561	E539	D447
C258	T235	A170	A565	S543	H451
V261	V238	T173	W610	W587	W489
Y262	Y239	V174	Y616	Y593	Y495
G366	A339	I261	W582	W657	W558
P367	P340	Q262	F726	F699	F601
V368	V341	P263	C730	C703	F605
L372	F345	Y267	I732	I705	L607
N373	C346	A268	Y734	Y707	Y609
Y410	T384	A306	Y737	Y710	Y612
N411	N385	S307			

Table 2. The supposititious residues of OSC, CAS and SHC close to the putative active site by sequence alignment.

1.7 Research Goal

Recent studies of ERG7, via three-dimension crystal structure analyses coupled with bioorganic and mutagenesis data, have provided deeper insight into the catalytic mechanism, the diversity of product profiles, and functional role of specific residues. The aromatic hypothesis suggested that the aromatic acid residues were highly conserved to stabilize cationic intermediates in the active site cavity of oxidosqualene cyclase during ring formations. The sequence alignment analysis revealed that the Tyr510 and Phe699 residues were conserved in the homologous cyclases, which might imply that the functional roles for cyclization/rearrangement cascades.

In previous papers, the Tyr420 residue (corresponding to Tyr510 of *S.cerevisiae* ERG7) in squalene-hopene cyclase (SHC) was determined to stabilize carbocation intermediate at C-10 during B-ring formation. In addition, we recently identified five single-point mutations within the *A. thaliana* CAS enzyme that lead to the production of lanosterol and supplement of the growth of a *S. cerevisiae* *erg7*-deficient strain. As part of this study, we determined that a Tyr532His (corresponding to Tyr510 in *S. cerevisiae* ERG7) mutation in *A. thaliana* CAS produced both lanosterol and the monocyclic product achilleol¹⁴. Accordingly, amino acid residues 509–513(TYEKI) of ERG7 were subjected to determine the effect on the cyclization/rearrangement mechanism via the alanine-screen mutagenesis^{15,18,19,33,44}. Moreover, in human OSC structure, a proton donor via a hydrogen-bonding network between the hydroxyl group of Tyr503 and His232 was mentioned for the final deprotonation step in lanosterol formation. Finally, the mutations of Tyr510 to Ala, Lys, Trp and His lead to the production of prematurely truncated and alternative deprotonation compounds. The findings suggested that the position of Tyr510 on *S. cerevisiae* ERG7 might play a functional role for the stabilization of C8/C10 lanosteryl cation as well as

monocyclic cation.

In the part of Phe699, the site-directed mutagenesis experiment on Phe601Ala (corresponding to Phe699 in *S. cerevisiae* OSC) in SHC was carried out to determine the catalytic activity and product profile. The isolation and characterization of multiple triterpenes, including altered deprotonation and rearrangement products implied the instability of protosterol carbonic cation in catalytic mechanism. Thoma *et al.* proposed, from the crystal structure of human OSC, that His232 and Phe696 (corresponding to His234 and Phe699 of *S. cerevisiae* ERG7, respectively) are positioned near the C-13 and C-20 positions of lanosterol and for π -cation interaction with the C-13 anti-Markovnikov tricyclic cation. We previously performed site-saturated mutagenesis experiments on the His234 residue of ERG7 and isolated diverse product profile, indicating that His234 of ERG7 plays a key role in stabilizing various carbocation intermediates and guiding the deprotonation reactions. A detailed investigation of the structural model suggested different spatial orientation of Phe699 relative to that of His234, although both residues are proximal to the C/D ring region. Therefore, it is tempting to investigate the influence of Tyr510 and Phe699 residues on structure-function relationships with the enzyme active site cavity.

In this study, the site-saturated mutagenesis of Tyr510 and Phe699 residues of *S. cerevisiae* ERG7 were performed to determine the dual functions in cyclization and rearrangement reactions. The results were described into two parts: part A is for Tyr510 and part B for Phe699.

Chapter 2 Materials and Methods

2.1 Chemicals and Reagents

Acetone (Merck)

95% Alcohol (Merck)

Adenine (Sigma)

Agarose-LE (USB)

Ampicillin sulfate (Sigma)

Anisaldehyde (Merck)

Bacto™ Agar (DIFCO)

D-Sorbitol (Sigma)

Dichloromethane (Merck)

Dimethyl sulfoxide (MP Biomedicals)

DNA 10Kb Ladder (Bio Basic Inc., Taiwan)

Ethyl acetate (Merck)

Ether (Merck)

Ergosterol (Sigma)

G418 (Gibco)

Glucose (Sigma)

Hemin Chloride (Merck)

Hexane (Merck)

Hisidine (Sigma)

LB Broth, Miller (DIFCO)

Lysine (Sigma)

Methioine (Sigma)

dNTP Set, 100mM Solutions (GE Healthcare)



Primers (Bio Basic Inc., Tanwan)
Potassium hydroxide (Merck)
Pyrogallol (Merck)
Restriction enzyme (New England BioLabs Inc.)
Seasand (Merck)
Silica gel (Merck)
Silver nitrate (Merck)
Sodium sulfate (Merck)
SYBR[®] Green I (Roche)
TLC plate (Merck)
Tryptophan (Sigma)
Tween 80 (Merck)
Trypton (DIFCO)
Yeast Extra (DIFCO)
Yeast Nitrogen Base w/o amino acid (DIFCO)
Uracil (Sigma)



2.2 Bacterial, yeast strains, plasmids

Escherichia coli XL-Blue (Novagen)

leu-Δ1 lys2-801 trp1-Δ63 ura3-52 hem1Δ::Kan^R)

pRS314Wt (a shuttle plasmid between bacterial and yeast contains wild type ERG7 gene, New England BioLabs)

TKW14C2 (a yeast strain, MAT_a or MAT_α ERG7 Δ :: LEU2 *ade2-101 his3-Δ200*)

2.3 Kits

BigDye[®] Terminator v3.1 Cycle Sequencing Kit (Applied Biosystems)

GFX[™] PCR DNA and Gel Band Purification Kit (GE Healthcare)

Plasmid Miniprep Purification Kit (GeneMark)

2.4 Equipments

ABI PRISM[®] 3100 Genetic Analyzer (Applied Biosystems)

Allegra[™] 21R Centrifuge (Beckman Coulter)

Avanti[®] J0E Centrifuge (Beckman Coulter)

Colling Circulator Bath Model B401L (Firstek Scientific)

Centrifuges 5415R (Eppendorf)

DU 7500 Spectrophotometer (Beckman Coulter)

Electrophoresis Power Supply EPS 301 (GE healthcare)

GeneAmp[®] PCR System 9700 Thermal Cycler (Applied Biosystems)

Hoefer[®] HE 33 Mini Horizontal Submarine Unit (GE Healthcare)

Kodak Electrophoresis Documentation and Analysis System 120 (Kodak)

Orbital Shaking Incubator Model-S302R (Firstek Scientific)

Pulse Controller (BioRad)

Rotary Vacuum Evaporator N-N Series (EYELA)

Steritop[™] 0.22µm Filter Unit (Millipore)

2.5 Solution

Ampicillin stock solution (100mg/mL)

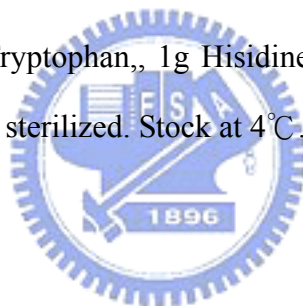
Dissolve 1g ampicillin sulfate in 10 mL ddH₂O. Filter through 0.22μm pore size filter and stock at -20°C.

50X TAE buffer

Dissolve Tris base 242g, acetic acid 57.1 mL, and 0.5 M EDTA in 1 L dH₂O and adjust to pH 8.5. Dilute to 1X with dH₂O and adjust to pH 7.5~7.8 before use.

50X ALTHMU solution

1g Adeine, 1.5g Lysine, 1g Tryptophan,, 1g Hisidine, 1g Methonine, 1g Uracil was dissolved in 500mL dH₂O and sterilized. Stock at 4°C.



50X ALHMU solution

1g Adeine, 1.5g Lysine, 1g Hisidine, 1g Methonine, 1g Uracil was dissolved in 500mL dH₂O and sterilized. Stock at 4°C.

50% Glucose solution

500g glucose was dissolved in 1 L dH₂O and sterilized.

80% Glycerol solution

80 mL glycerol was added in 20 mL dH₂O and sterilized. Stock at 4°C.

LB medium

25g LB Broth was dissolved in 1 L dH₂O and sterilized.

LB plate

25g LB Broth and 20g Bacto™ Agar was dissolved in 1 L dH₂O and sterilized. The sterile LB agar was poured and dispersed in Petri dishes before it coagulates.

G418 stock solution (1g/mL)

Dissolve 500mg G418 in 500μL sterile dH₂O. Stock in darkness at room temperature.

SD medium

6.7g Yeast nitrogen base was dissolved in 1 L dH₂O and sterilized.

20% EA developing solution

Add 20 mL ethyl acetate to 80 mL hexane and mix it.

TLC staining solution

40mL of conc. H₂SO₄ is added (slowly!) into ethanol 800mL, followed by acetic acid 12mL and anisaldehyde 16mL.



1M sorbitol solution

172.2g D-sorbitol was dissolved in 500 mL dH₂O and sterilized. Stock at 4°C.

5X sequencing buffer

Dissolve 4.85g Tris base and 0.203g MgCl₂ in 100 mL dH₂O and adjust to pH 9. Stock at 4°C.

10X SYBR Green solution

10000X SYBR Green was diluted to 10X with DMSO. Stock in darkness.

6X DNA loading dye

0.25% bromophenol blue and 30% glycerol in ddH₂O. Stock at -20°C.

Heme solution

0.5g hemin chloride was dissolved in 250 mL 0.2N potassium hydroxide and thus mixes it with 250 mL 95% alcohol in aseptic condition. Stock at room temperature in darkness.

Ergosterol supplement solution

1g Ergosterol was dissolved in 250 mL 95% alcohol and thus mixes with 250 mL Tween 80 in aseptic condition. Stock in darkness at room temperature.

ALHMU/Heme/Ergosterol plate

0.67g yeast nitrogen base, 2g Bacto™ Agar was dissolved in 100 mL dH₂O and sterilized. Add 2 mL 50X ALHMU solution, 4 mL 50% glucose solution, 2 mL heme solution, 2 mL ergosterol supplement solution, and 100μL G148 stock solution into the sterile SD medium. Then the mixture was poured and dispersed in Petri dishes before it coagulates. All of steps are in aseptic condition and stock in darkness at 4°C.

2.6 Construction of Mutants

2.6-1 Site-Directed Mutagenesis of $ERG7^{Y510X}$ and $ERG7^{F699X}$

Mutagenesis of Tyr510 and Phe699 in the wild type *ERG7* gene was performed using the QuickChange site-directed mutagenesis kit. The mutagenic oligonucleotide primers for Tyr510 are WHYOSCY510X1-*BamH* I, WHYOSCY510X2-*BamH* I, WHYOSCY510CF1-*BamH* I, WHYOSCY510CF2-*BamH* I, WHYOSCY510IMDF1-*BamH* I, and WHYOSCY510IMDF2-*BamH* I. The mutagenic oligonucleotide primers for Phe699 are WHYOSCF699X1-*Pvu* II, WHYOSCF699X2-*Pvu* II, WHYOSCF699CW1-*Pvu* II, WHYOSCF699CW2-*Pvu* II, WHYOSCF699INDEQ1-*Pvu* II, and WHYOSCF699INDEQ2-*Pvu* II (see Appendix 1). Each PCR reaction contains: 0.8mM of each dNTP, 100 ng of pRS314Wt plasmid as template, 1X *Pfu* polymerase buffer, 10 μ L of each primer, 2.5 U *Pfu* polymerase and ddH₂O to the final volume of 50 μ L. The reaction mixture was denatured at 95°C for 2 min, and then run for 18 cycles of denaturizing at 95°C for 30 sec each, annealing at 50~55°C for 1 min, with an extension at 68°C for 16 min (Table 3). The PCR products were incubated with *Dpn* I at 37°C for 3 hours to digest the parental supercoiled DNA. The resulting products were combined with 1 X SYBR Green and 1X DNA loading Dye and loaded onto 0.8% agarose gel with 0.5X TAE buffer. The gel with the PCR product mixtures was performed at 120Volt for 20 min and autoradiographed by Kodak Electrophoresis Documentation and Analysis System 120.

Table 3. Reaction conditions and cycling parameters for PCR mutagenesis reaction

pRS314WT plasmid	1
Primer 1 (10 μ M)	1
Primer 2 (10 μ M)	1
dNTP mix (2.5mM each)	4
10X <i>Pfu</i> polymerase buffer	5
ddH ₂ O	37
<i>Pfu</i> polymerase	1
Total	50 (μL)

Segment	Cycles	Temperature	Time
1	1	95°C	2 min
2	18	95°C	30 sec
		50~55°C	1 min
		68°C	16 min
3	1	4°C	pause

2.6-2 Transformation and Enzyme Mapping

The QuickChange products were added with 100 μ L *E. coli* XL1-Blue competent cells and incubated on ice for 20 min. The cells were transformed by heatshock method for 1 min at 42°C following 1 min on ice. Then the cells were transferred to 1 mL Luria-Bertani (LB) medium immediately and shaken at 200 rpm for 1 hour at 37°C incubator. Then, the cells were centrifuged at 8000 rpm for 1 min and propagated on LB plate containing 100 μ g/mL ampicillin (LB_{amp}). Incubate plate overnight at 37°C. Pick the colonies and culture in 3 mL LB medium containing 100 μ g/mL ampicillin overnight at 37°C. The plasmid DNAs were isolated by Plasmid Miniprep Purification Kit, following the manufacturer instructions. The plasmid DNAs were then digested with *Bam*H I for Tyr510 mutants and *Pvu* II for Phe699 mutants to confirm the presence of the mutations.

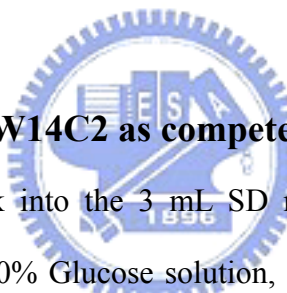
2.6-3 Sequence analysis of ERG7^{Y510X} and ERG7^{F699X} mutant gene

The exact substitution at Tyr510 and Phe 699 position were determined by sequence of the DNA by use of an ABI PRISM 3100 auto-sequencer. Nucleotide

sequencing was performed using the dideoxynucleotide chain-termination method with only one forward or reverse primers (described on Appendix 1). Sequencing reactions were carried out with BigDye[®] Terminator v3.1 Cycle Sequencing Kit, according to the manufacturer protocol. Briefly, each of sample was performed with 1 μ L each forward or reverse primer, 2 μ L plasmid DNA, 3 μ L 5X sequencing buffer, 1 μ L premix and ddH₂O to create a final volume of 50 μ L. The each of reaction was performed on the ABI PRISM[®] 3100 Genetic Analyzer, following the manufacturer's guidelines.

2.7 Transformation and Genetic selections ERG7 mutants

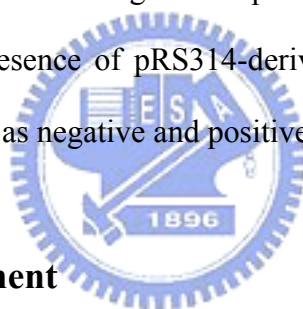
2.7-1 Preparation of TKW14C2 as competent cell



Pick the TKW14C2 stock into the 3 mL SD medium, containing 60 μ L 50X ALTHMU solution, 120 μ L 50% Glucose solution, 60 μ L Heme solution and 60 μ L ergosterol solution and then incubated at 30°C for two to three days. When the cell grew well, transferred it to 100 mL SD medium with the same condition and incubated at 30°C for 12 to 18 hours. After OD₆₀₀ reaches 1.0~1.5, the cells was centrifuged to collect at 3000 rpm, 10 min at 4°C and the supernatant was discarded. Add 35 mL aseptic ddH₂O to resuspend the pellet and centrifuge it at 3000 rpm, 10 min at 4°C repeated two times. Then add 25 mL 1 M D-sorbitol solution to resuspend the pellet and centrifuge it at the same condition. Finally, add 1000 μ L 1 M D-sorbitol into the pellet and resuspend it gently on ice for 5 min. The volume of 80 μ L competent cell was added into each of 1.5 mL microtube with 5 μ L mutated plasmid, respectively.

2.7-2 Transformation of mutated plasmid into TKW14C2

The mutated plasmids of ERG7^{Y510X} and ERG7^{F699X} were transformed into TKW14C2, an ERG7-deficient yeast strain, by electroporation using a GenPulser with Pulse Controller (BioRad). Pipet total of electrocompetent cell with plasmid DNA onto drop and flick cuvette to settle DNA + cells mixture into bottom of cuvette. Set the conditions for transformation according to strains. For TKW14C2 cells, use 1.5k volt and the time constant should be 3-4 seconds. Dry off any moisture from cuvette outside and immediately place cuvette in white plastic holder. Slide holder into position and zap cells. If you hear a high constant tone, immediately add the 0.5 mL of D-sorbitol solution to cells. Aliquots of 120 μ L of each culture were plated onto SD+Ade+Lys+His+Met+Ura+hemin+Erg+G418 plates, and incubated for three to five days to select for the presence of pRS314-derived plasmids. The pRS314 and pRS314WT were transformed as negative and positive control, respectively.



2.7-3 Ergosterol supplement

Several colonies from each of the plates were picked to reselect on two kinds of selective plates, SD+Ade+Lys+His+Met+Ura+hemin+Erg+G418 and SD+Ade+Lys+His+Met+Ura+hemin+G418. The transformants were incubated three to five days at 30°C. Ergosterol supplement is a selection marker for functional complementation of cyclase in ERG7 mutants.

2.8 Extracting lipids and characterizing mutant product profiles

2.8-1 Cell culture and extraction

Two and half liter cultures of TKW14C2[pERG7^{Y510X}] and TKW14C2[pERG7^{F699X}] transformants were grown in SD+Ade+Lys+His+Met+Ura+Hemin(+Erg) medium at 30°C with shaking (150 rpm) for seven to ten days. The cells were harvested by centrifugation, washed, and saponified with 200 mg pyrogallol by refluxing them in 250 mL of a 15% KOH/ 50% EtOH for 2 hours. Three volumes of petroleum ether were added to extract the nonasponifiable lipid. The petrol extract was washed with water, dried over with anhydrous sodium sulfate, filtered and dried thoroughly in a rotary evaporator. The extract was fractionated by silica gel column chromatography using a 19:1 hexane/ethyl acetate mixture. Each of fractions was checked by thin layer chromatography and divided into five areas, according to OS, LA up, LA, LA down, and Erg region. The fractions of LA up, LA, and LA down sections were dried to perform on GC and GC/MS analysis.

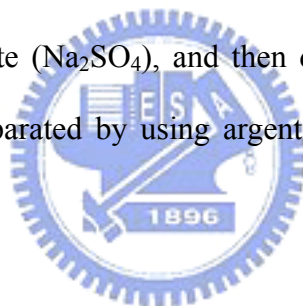
2.8-2 GC and GC/MS conditions

GC analyses were performed with a Hewlett-Packard model 5890 series II or Agilent 6890N chromatography equipped with a DB-5 column (30 m x 0.25 mm I.D., 0.25 µm film; oven gradient at 50°C for 2 min, and then 20°C per min until 300°C, held at 300°C for 20 min, 300°C injector; 250°C interface; 1/40 split ratio using helium carrier gas at 13 psi column head pressure). GC/MS was performed on a Hewlett-Packard model 5890 II GC (J & W DB-5MS column, 30 m x 0.25 mm I.D., 0.25 µm film; oven 280°C, injector 270°C, GC-MS transfer line: 280°C) coupled to a TRIO-2000 micromass spectrometer.

2.9 Isolation of mutant products by using acetylation modification

2.9-1 Acetylation modification and the alkaline hydrolysis reaction

The acetylation modification of triterpene alcohols were performed to alter the polarity of mutant products, following the previous paper. The dry triterpene alcohol fraction was first dissolved in 2 mL pyridine solvent, and then 1 mL acetic anhydride was added into the reaction. The reaction was performed with the closed system in the hood and stirred for 12-16 hours at room temperature. The acetylation reaction was monitored by TLC analysis per 4 hours. After 16 hours, 10 mL water was added to terminate the acetylation reaction, and then three times extractions with 20 mL dichloromethane (CH_2Cl_2) were carried out. The total organic phase was collected and dried over with sodium sulfate (Na_2SO_4), and then dried by rotary evaporator. The acetylation products were separated by using argentic column chromatography and analyzed by GC-MS.



2.9-2 Argentic colum chromatography

8.6g of silver nitrate was dissolved in 50 mL of distilled water. 25g of silica gel was slowly added to this solution and hand mixed. The adsorbent was dried over than 16 hours in an oven at 110°C . The argentic silica gel was packed a slurry in hexane to from a column about 20cm. The mixture of acetylated products was loading onto the argentic column and separated with 1:24 ether/hexane. The fractions were analyzed by GC-MS.

2.9-3 Deacetylation reaction of the modified products

The dry triterpene alcohol fraction was dissolved in 10 mL methanol, and 0.5g potassium hydroxide (KOH) was added into the reaction. The reaction was performed

with the closed system in the hood and stirred for 12-16 hours at room temperature. The deacetylation reaction was monitored by TLC analysis. After 16 hours, the reactant was dried by rotary evaporator and then 10 mL water was added to dissolve potassium hydroxide. The deacetylated products were thrice extracted with dichloromethane. The total organic phase was collected and dried over with anhydrous sodium sulfate (Na_2SO_4), and then dried thoroughly in a rotary evaporator. The deacetylated products were separated by silica gel column chromatography using 19:1 hexane/ethyl acetate (HPLC level) mixture. The structures of finally novel products from *sceERG7*^{F699M} characterized and identified by NMR spectroscopy (¹H, ¹³C, DEPT, COSYDEC, HSQC, HMBC, and NOE).

2.10 Molecular modeling

Molecular-modeling studies were performed, using the Insight II Homology program with the X-ray structure of lanosterol-complexed human OSC as the template. The MODELER program is designed to extract spatial constraints such as stereochemistry, main-chain and side-chain conformation, distance, and dihedral angle from the template structure. The resulting structure was optimized using an objective function that included spatial constraints and a CHARMM energy function. The objective function combines free energy perturbation, correlation analysis, and combined quantum and molecular mechanism (QM/MM) to obtain a better description of molecular level structure, interactions, and energetics. The homologous model structure, with the lowest objective function, was evaluated further using the Align2D algorithm for sequence-structure alignment.

Chapter 3 Results

Part A: The functional analysis of tyrosine 510 within *Sce*ERG7

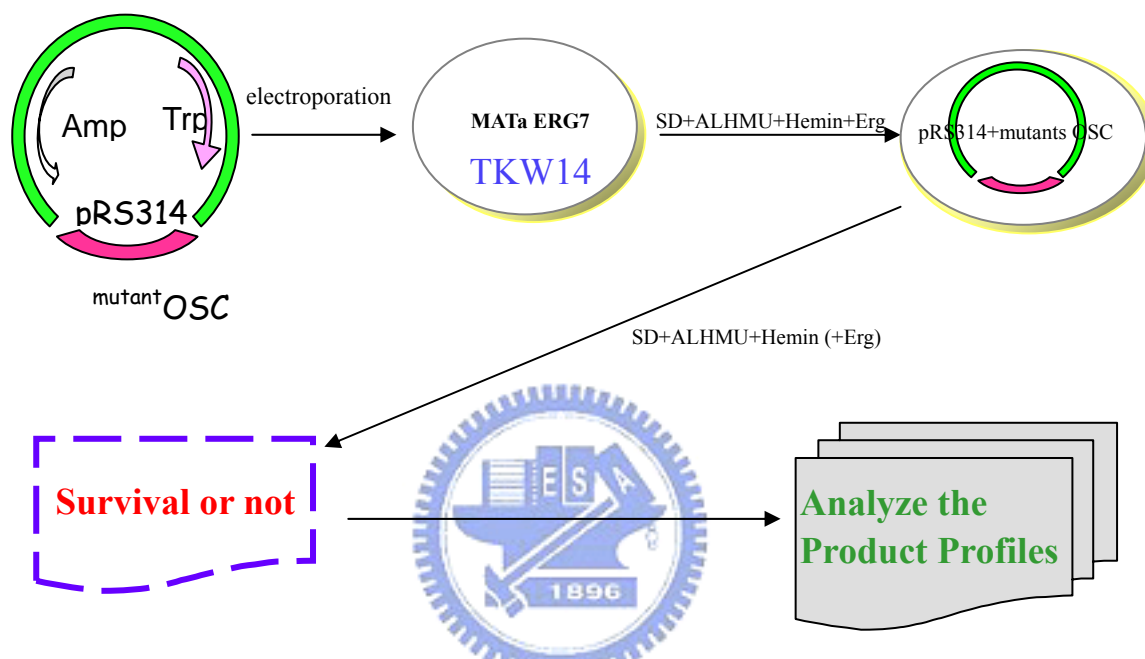
3A.1 Site-saturated mutagenesis of Tyr510

The saturated mutations of Tyr510 within oxidosqualene-lanosterol cyclase from *Saccharomyces cerevisiae* were constructed employing QuickChange Site-Directed Mutagenesis, and mapped by restriction enzyme *Bam*H I. All mutations were confirmed by DNA sequencing using the dideoxy chain-termination method and ABI PRISM 3100 autosequencer. The recombinant plasmids were electroporated into the yeast ERG7-deficient strain, TKW14C2, selected for growth on SD+Ade+Lys+His+Met+Ura+Hemin+Erg+G418 plates, and reselected on SD+Ade+Lys+His+Met+Ura+Hemin+G418 to determine whether the ERG7^{Y510X} mutant protein could complement the cyclase deficiency of TKW14C2. The yeast cells derived with ERG7^{Y510X} mutants that failed to complement cyclase function would not survive on the plates without ergosterol supplement (see Fig. 3-1). Among the various mutants, the Tyr510Lys, Tyr510Arg, Tyr510Thr, Tyr510Pro and Tyr510Trp mutations failed to complement the ERG7 disruption strain, TKW14C2, when in the absence of exogenous ergsterol (Table 4). The finding suggested that the different side chain substitution of Tyr510 might influence the stability of *S. cerevisiae* ERG7, and abolish catalytic activity.

Next, the products generated by the ERG7^{Y510X} mutants were analyzed, following the nonsaponifiable lipid extraction and silica gel column separation. The ERG7^{Y510X} mutants produced from monotonous to diverse product profiles with a molecular mass of $m/z = 426$, analyzing by GC-MS. Based on the retention time and mass spectrum of

products, all of the compounds including achilleol A, camelliolC, (13 α H)-isomalabarica-14(26),17,21-trien-3 β -ol, lanosterol and parkeol were identified. The data of product profiles ratio were shown on Table 5.

Fig. 3-1: The strategy of survival selection experiment.



The replacements of tyrosine with arginine, proline and threonine failed to generate product with molecular mass of $m/z = 426$. The side chain of these amino acids might be steric barrier in the enzyme active site cavity. Most of the $ERG7^{Y510X}$ mutants, expressing in the TKW14C2, produced the truncated compounds from the C-10 and C-14 cation intermediate as well as alternative deprotonation products, parkeol. The finding suggested that the position of tyrosine 510 might be closed to C8/C9 for final deprotonation and affect cation stabilization at the C10 and C14 position for monocyclic and tricyclic product, respectively.

The isolation of (13 α H)-isomalabarica-14(26),17,21-trien-3 β -ol suggested that the occasional misfolding leading to the tricyclic product in $ERG7^{Y510}$ mutants might

result from the mobility of aryl ring and the change of the hydrogen-bond network. Alternatively, the steric and electronic changes might slightly retard the substrate folding during the D-ring formation, while allowed the early deprotonation at C-14 carbocation intermediate position. The mutations of Tyr510 might affect cyclization to achilleol A as well as deprotonation to lanosterol and parkeol, possibly through partial disruption of transient dipole interactions between carbocationic intermediates and the hydroxyl group of the aromatic ring of Tyr510.

Table 4. Site-Saturated Mutagenesis of Tyr510 and ergosterol complement selection.

Substitutions of Tyr510	Sequence confirmation	Genetic selection	Conter-selection	New product
Gly	ok	Live	Live	+
Ala	ok	Live	Live	+
Val	ok	Live	Live	+
Leu	ok	Live	Live	+
Ile	ok	Live	Live	+
Asp	ok	Live	Live	+
Asn	ok	Live	Live	+
Glu	ok	Live	Live	+
Gln	ok	Live	Live	+
His	ok	Live	Live	+
Lys	ok	Die	Die	+
Arg	ok	Die	Die	-
Ser	ok	Live	Live	+
Thr	ok	Die	Die	-
Cys	ok	Live	Live	+
Met	ok	Live	Live	+
Phe	ok	Live	Live	+
Trp	ok	Die	Die	+
Pro	ok	Die	Die	-

According to the crystal structure of human OSC, Tyr503 provides hydrogen-bond network to His232 (of human OSC) considered as the closest residue for the final deprotonation step at the C-8 cation in lanosterol formation. In addition, our previous study on the site-saturated mutagenesis of His234 showed that the substitutions at the His234 position might influence the C-13 and C-20 positions as well as the C-14 anti-Markovnikov secondary cation during the rings formation²⁴. By this study, simulated substitution of ERG7^{H234} with other amino acid residues showed that this position affected steric or electrostatic interactions between the cationic intermediate and the active site side chain. On the other hand, the substitutions of His234 with small nonpolar hydrophobic residues resulted in facilitating the production of polycyclic products such as parkeol, protosta-12,24-dien-3 β -ol, and protosta-20,24-dien-3 β -ol, but interfered with achilleol A formation. Interestingly, substitutions of larger or basic amino acids on Tyr510 tended to produce monocyclic products, whereas the small or acidic amino acids substitutions tended to produce polycyclic products. For example, the substitutions of Tyr510 with acidic group residues, including Asp, Asn, Glu, and Gln might increase the electronic density to attract the carbocation intermediate near positions C-8 and C-9. These mutants influenced the final deprotonation at C-9 cation and produced parkeol. The substitutions of Tyr510 with basic group or large amino acid such as His, Lys, Arg and Trp might cause the steric or electronic repulsion to His234 residue. The mutants increased the production of monocyclic compounds, achilleol A and camelliol C, *via* the alternative deprotonation of the carbocation intermediates at C-10 position. To our surprise, the ERG7^{Y510W} mutant produced almost monocycle but no tricyclic or tetracyclic products. In contrast, the ERG7^{H234W} mutant generated almost one hundred percentage of parkeol without other cyclization products. These findings suggested that the steric influence involved in the bulk substitution of side chain might disrupt

the proper binding orientation or the coordinative interaction between these important residues of active site cavity.

Table 5. The ratio of triterpene product profiles from *Sce*ERG7^{Y510X} mutants.

Substitution of Y510		achilleol	isomalabarica	LA	parkerol	camelliol	No product
		A				C	
	Gly	15	17	27	41	-	
Aliphatic group	Ala	27	0	39	34	-	
	Val	4	17	38	41	-	
	Leu	0	26	74	0	-	
	Ile	4	11	78	7	-	
Acidic and amide group	Asp	9	11	40	40	-	
	Asn	5	9	9	77	-	
	Glu	6	27	18	49	-	
	Gln	5	26	14	55	-	
Basic group	His	45	24	5	26	-	
	Lys	87	0	0	0	13	
	Arg						V
Hydroxyl-group	Ser	0	4	40	56	-	
	Thr						V
Sulfur-containing	Cys	0	67	33	0	-	
	Met	1	15	43	41	-	
Aromatic group	Phe	4	10	50	36	-	
	Trp	94	0	0	0	4	
Imino	Pro						V
H234W	Y510V	2	8	90	-	-	
H234W	Y510W	99	-	-	-	1	

According to the homology model of *S. cerevisiae* OSC (Fig. 3-2), the Tyr510 residue located at the same side with His234 in oxidosqualene cyclase cavity might participate in the cyclization and/or skeletal rearrangement cascades in lanosterol formation. We constructed the ERG7^{Y510V/H234W} and ERG7^{Y510W/H234W} double mutant

and analyzed the product profiles ratio from these two mutants (Table 5). The dramatically opposing result of the product profile ratios revealed that the side chain group of either Tyr510 or His234 would dramatically influence the cyclization from oxidosqualene to (13 α H)-isomalabarica-14(26),17,21-trien-3 β -ol and lanosterol. The results of product profiles ratio from these double mutants could be explained by the stereochemistry of three-dimension structure in molecular modeling (Fig. 3-2).

3A.2. The result of homology modeling of *S.cerevisiae* OSC

The homology model of the *S. cerevisiae* ERG7 was created by using the Insight-II Homology program with the X-ray structure of lanosterol-complexed as the template. The observed hydroxyl group of Tyr510 located at a distance of about 5.42 Å to the C10 cation of lanosterol; this distance agreed with the dipoles for observed aromatic amino acid residues at distance of 3.5 to 5.5 Å in the lanosterol-bound OSC complex¹⁵. Therefore, the mutations of ERG7^{Y510X} might influence cyclization as well as deprotonation step in the reaction cascades.

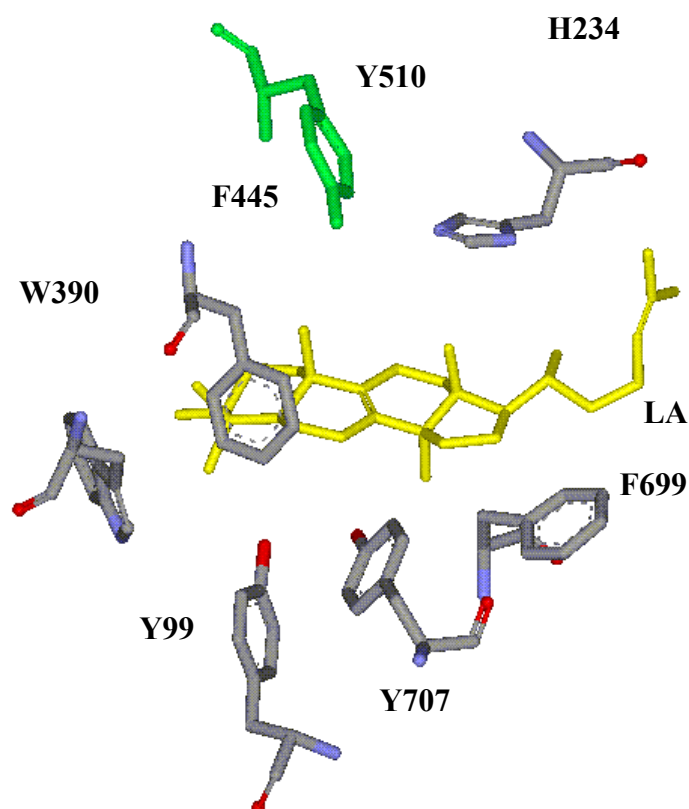
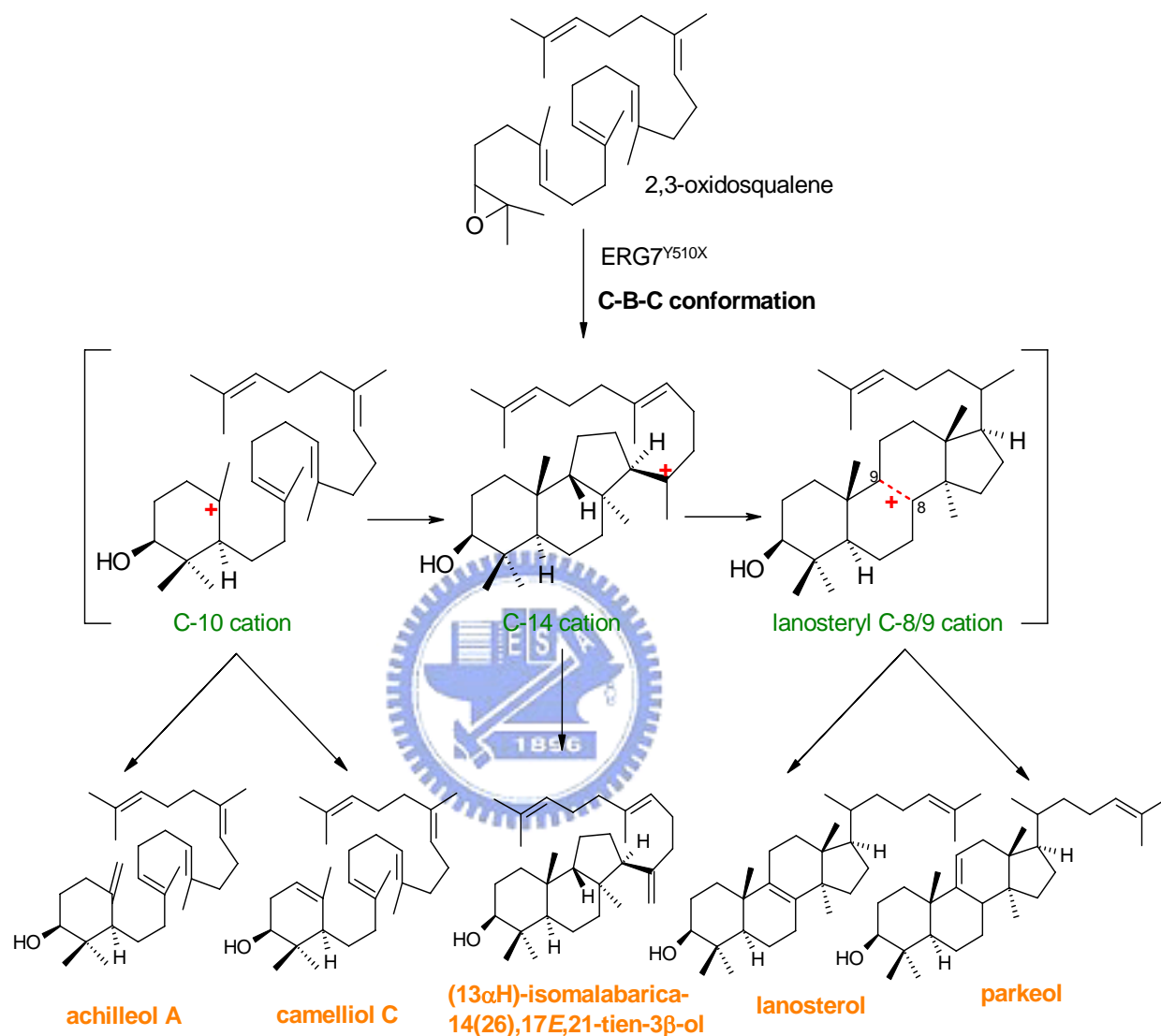


Fig. 3-2 Local view of the homology modeled *S.cerevisiae* ERG7 structure, based on the lanosterol-bound human OSC X-ray structure.

In considering the critical role of Tyr510 in deprotonating step to form lanosterol, these Tyr510 mutants produced predominantly lanosterol despite loss of the deprotonating hydroxyl group. The new hydrogen-bond network formed between the different substitutions of the Tyr510 and His234 residues might be formed while His234 was close enough to H-9 for direct deprotonation (Fig. 3-2). A modified hydrogen-bond network might cause the steric changes to arrest the D-ring formation, and affect the stability of the C-14 cation intermediate.

In summary, both achilleol A and camelliol C were identified as evidence for premature truncation of C10 cation intermediate after A-ring formation. Then, the substrate conformer was cyclized to form a tricyclic Markenikov C-14 cation and subsequently abstracted C-26 proton to yield (13 α H)-isomalabarica-14(26),17,21-trien-3 β -ol as the end product. This finding provided a support for the hypothesis that the formation of lanosterol from oxidosqualene in ERG7-catalyzed cyclization/rearrangement cascade proceeded *via* the anti-Markovnikov 6-6-5 tricyclic cation (Fig. 3-3). In addition, with the migration of two methyl groups, the lanosteryl C-8 cation intermediate was generated to form lanosterol and parkeol from the ERG7^{Y510X} mutants (Scheme III). In addition, the identification of ERG7^{Tyr510} showed its importance for cyclase activity and controlling the catalytic function of oxidosqualene cyclases during cyclization/rearrangement cascades. Finally, the isolation of the tircyclic (13 α H)-isomalabarica-14(26),17,21-trien-3 β -ol provided a direct evidence that the expansion of C-ring was proceeding *via* the C-14 anti-Markovnikov secondary cation. The anti-Markovnikov addition occurred during the expansion of C-ring and D-ring in lanosterol formation suggested that the active site cavity residues might lower the activation energy to catalyze the cyclization reaction.

Scheme III . Proposed cyclization/rearrangement pathway of oxidosqualene in TKW14C2 expressing ERG7^{Y510X} site-saturated mutagenesis.



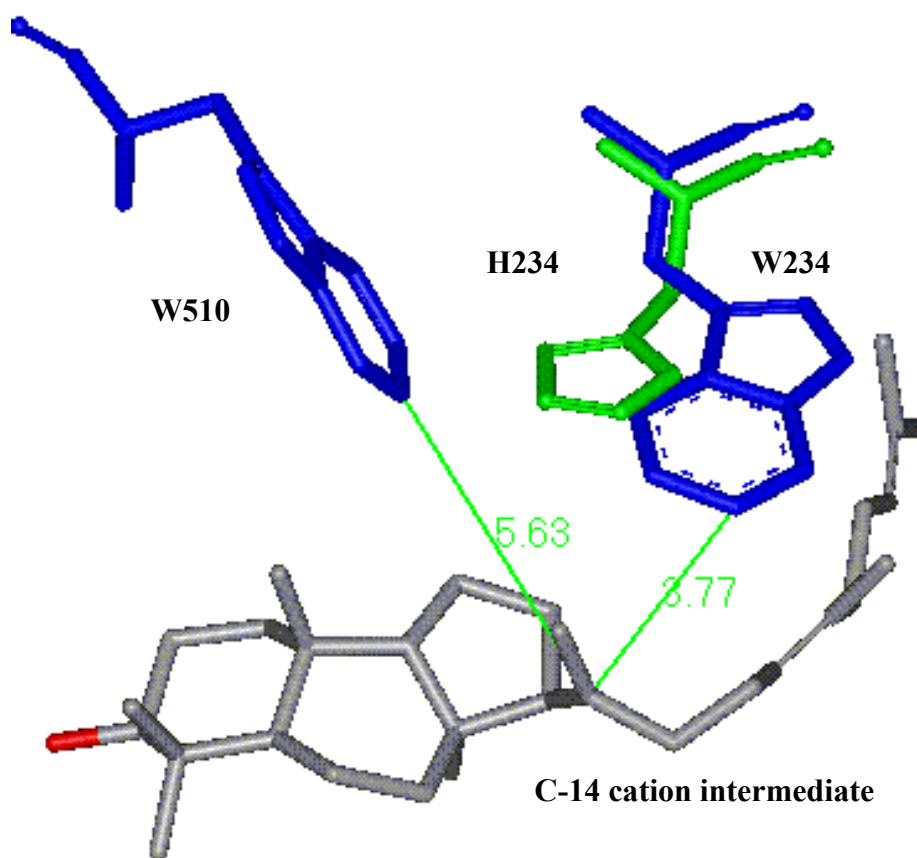
3A.3. Double mutagenesis of $ERG7^{H234W/Y510V}$ and $ERG7^{H234W/Y510W}$

Based on the three-dimensional structure of lanosterol-complexed human oxidosqualene cyclase, the residues of Tyr503 (corresponding to Tyr510 in *S. cerevisiae* ERG7) and His232 (corresponding to His234 in *S. cerevisiae* ERG7) were positioned at the same side of lanosterol. The side-chain of Tyr503 was in an appropriate position and orientation to stabilize C6 and C10 cation intermediate, whereas His232 side chain was positioned to stabilize the anti-Markovikov secondary cation at C14. However, the hydrogen-bonded network between the hydroxyl group of Tyr510 and His234 would play an important role for the final deprotonation step (Fig. 3-2).

In order to find the relationship between His234 and Tyr510, we designed the primers to construct the double mutations of *S. cerevisiae* ERG7 employing QuickChange Site-Directed Mutagenesis. We have constructed two double mutations plasmid, the $ERG7^{H234W/Y510V}$ and $ERG7^{H234W/Y510W}$ and then transformed into the TKW14C2 strain, following the protocol described in chapter 2. The products generated by the mutants were identified *via* the retention time and mass spectrum by GC-MS. The substitutions of Tyr510 with Trp or Val and that of His234 with Trp might affect the tendency of product profiles from ERG7 mutants. For example, the $ERG7^{H234W/Y510V}$ mutant produced more polycyclic products like lanosterol and isomalabarica, but the $ERG7^{H234W/Y510W}$ mutant produced only monocyclic achilleol A in GC-MS analysis. Compared with the product profiles from the $ERG7^{H234W}$ and $ERG7^{Y510W}$ mutants, the replacement of tyrosine with tryptophan led to the truncated product, but not the alternative deprotonation one. The impact on the substitutions of both residues could be described in steric conformation change through the homology modeling with Insight II program. The homology modeling of $ERG7^{H234W/Y510W}$

showed that the position of His234 was off from the original location within the active site cavity of oxidosqualene cyclase (Fig. 3-4). The steric and stereochemistry influence on the conformation change of the ERG7^{Y510W/H234W} mutant might provide an observation to suppose the diversity of product profiles from the mutants.

Fig. 3-4. The modeling of ERG7^{H234W/Y510W} mutant with C-14 cation intermediate, green means wild type His234, blue means Trp234 mutant.



Part B: The functional analysis of phenylalanine 699 within

*Sec*ERG7

3B Site-saturated mutagenesis of Phe699

The saturated mutations of phenylalanine 699 within oxidosqualene-lanosterol cyclase from *Saccharomyces cerevisiae* were constructed by QuickChange Site-Directed Mutagenesis Kit and expressed in yeast strain TKW14C2 for *in vivo* assay. The TKW14C2 strain, a CBY57-derived HEM1 ERG7 double-knockout mutant, is only viable when supplied with exogenous ergosterol or complemented with oxidosqualene cyclase activity derived from ERG7^{F699X}. The genetic selection result showed that the F699X mutation resulted in inviability of TKW14[pERG7^{F699X}] mutants, except for Leu, Ile, His, Thr, Met, and Pro substitutions, when in absence of exogenous ergosterol (Table 6). This finding indicated the crucial role of Phe699 in the catalytic active site of *S. cerevisiae* ERG7. The products generated from the ERG7^{F699X} mutants were analyzed, following the nonsaponifiable lipid (NSL) extraction and the silica gel column separation. The ERG7^{F699X} mutants produced from monotonous to diverse product profiles with molecular mass of $m/z = 426$, analyzed by GC-MS. For example, the ERG7^{F699T} mutant produced a new novel compound as major product (>99.8%). In contrast, the replacement of Phe699 with Met leads to produce six novel products with a molecular mass of $m/z = 426$, including two compounds indistinguishable from authentic (13 α H)-isomalabarica-14(15)E,17E,21-dien-3 β -ol, and (13 α H)-isomalabarica-14(15)Z,17E,21-dien-3 β -ol, identified via the retention time and mass pattern on GC-MS. Interestingly, no altered deprotonation products of parkeol and 9 β -lanosta-7,24-dien-3 β -ol were observed in GC-MS analyses, from any of the mutants. In other ERG7^{F699X} mutants, including ERG7^{F699N}, ERG7^{F699K}, ERG7^{F699H}, and ERG7^{F699T} also produce these products except tricyclic products.

Table 6. Site-Saturated Mutagenesis of Phe699 and ergosterol complement selection

Substitutions of Phe699	Sequence check	Genetic selection	Counter-selection	New product
Gly	ok	Die	Die	-
Ala	ok	Die	Die	-
Val	ok	Die	Die	-
Leu	ok	Live	Live	-
Ile	ok	Live	Live	-
Asp	ok	Die	Die	-
Asn	ok	Die	Die	+
Glu	ok	Die	Die	-
Gln	ok	Die	Die	-
His	ok	Live	Live	+
Lys	ok	Die	Die	+
Arg	ok	Die	Die	-
Ser	ok	Die	Die	-
Thr	ok	Live	Live	+
Cys	ok	Die	Die	-
Met	ok	Live	Live	+
Tyr	ok	Die	Die	-
Trp	ok	Die	Die	-
Pro	ok	Live	Live	-

In order to separate and isolate the other unknown compounds, the products mixture was acetylated. The acetylation altered the compound polarity and change molecular mass from 426 to 468 (Fig. 3-4 and Fig. 3-5). By way of AgNO₃ impregnated silica gel chromatography, using 3% diethyl ether in hexane as mobile phase, three of the novel products were isolated from the compounds mixture.

Fig. 3-5. The mass spectrum of novel products form ERG7^{F699Met} mutant.

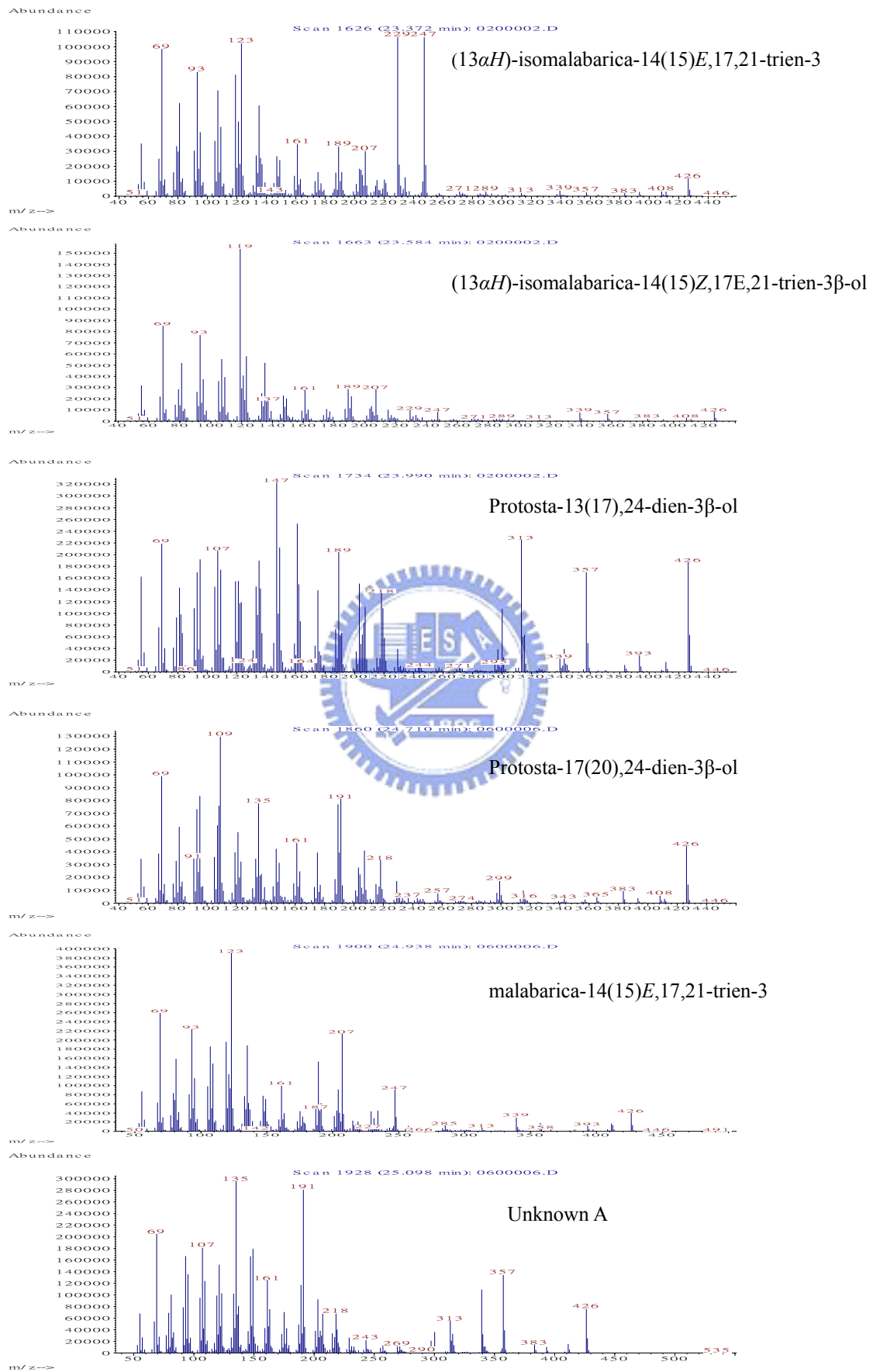
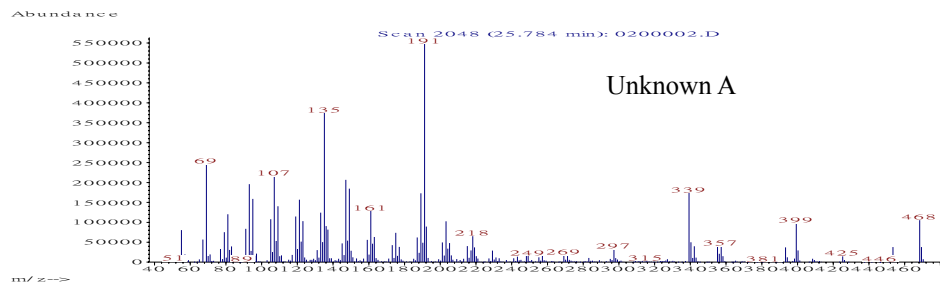
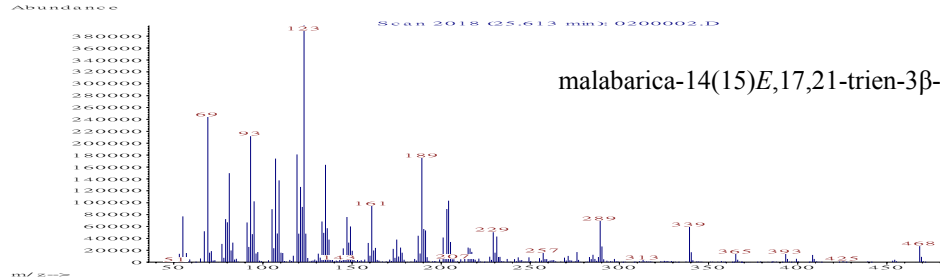
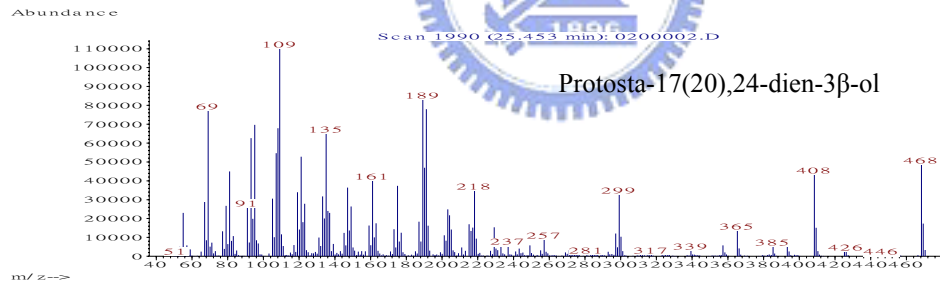
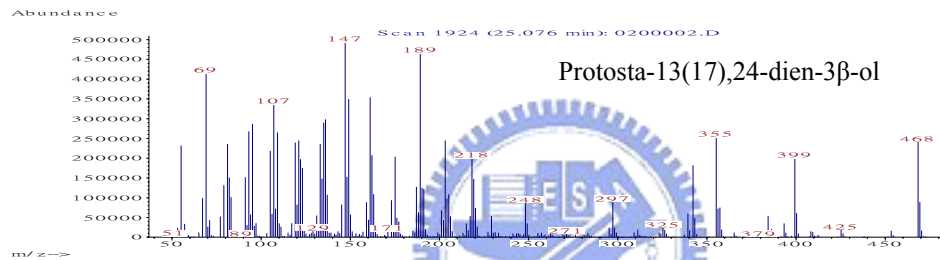
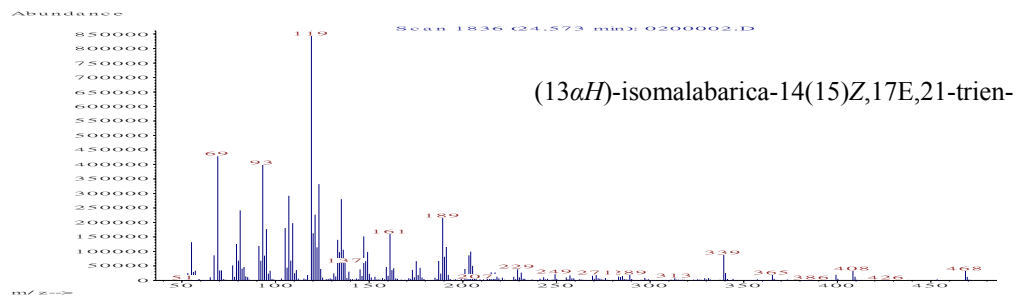
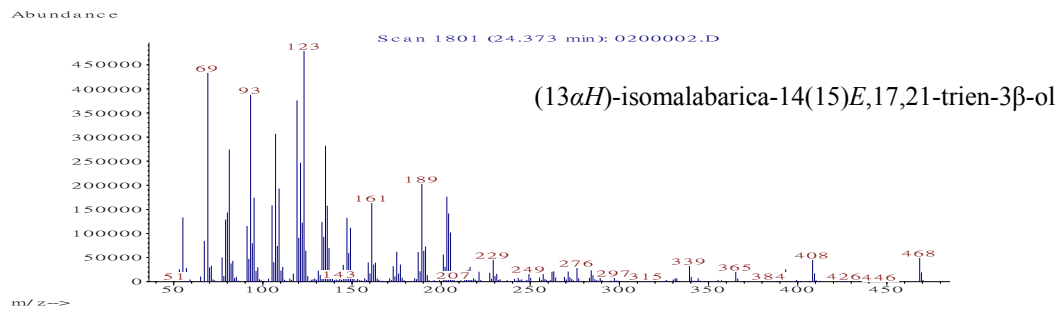
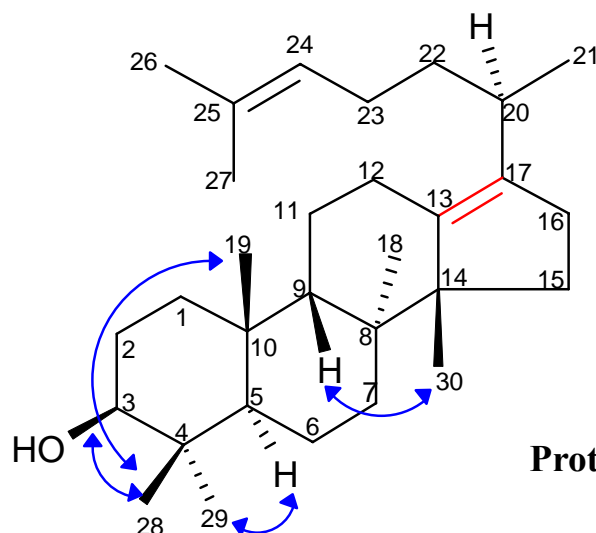


Fig. 3-6 The mass patterns of the acetylated compounds from ERG7^{F699Met} mutant.





Protosta-13(17),24-dien-3 β -ol (Fig. 3-7)

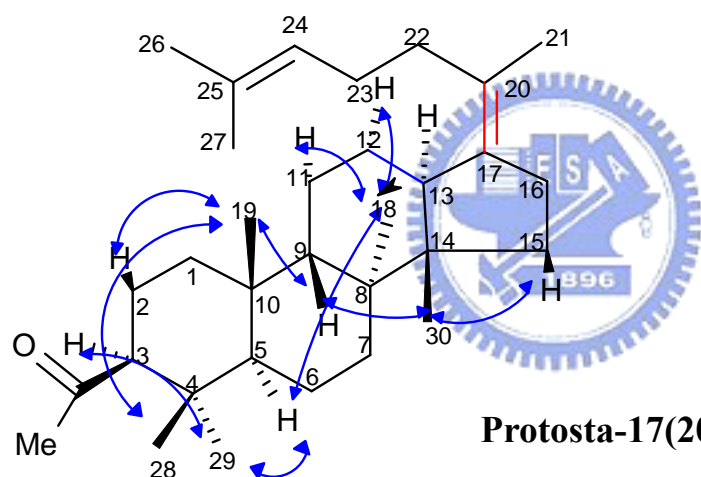
	^{13}C (δ)	^1H (δ)	^{13}C (δ)	^1H (δ)	^{13}C (δ)	^1H (δ)		
C-1	33.87	1.49,1.39	C-11	23.07	1.52,1.21	C-21	20.05	0.93,0.94
C-2	28.95	1.58,1.60	C-12	23.29	1.78,2.35	C-22	35.68	1.26
C-3	79	3.2,d, $J=6.89\text{Hz}$,3H	C-13	139.2	-	C-23	26.36	1.76,1.83
C-4	39.33	-	C-14	57.45	-	C-24	124.79	5.05
C-5	47.61	1.37	C-15	30.98	1.84,1.28	C-25	130.94	-
C-6	18.38	1.51,1.24	C-16	28.7	2.13,2.08	C-26	25.71	1.64
C-7	33.32	1.22,1.89	C-17	135.3	-	C-27	17.59	1.53
C-8	40.14	-	C-18	22.89	0.92	C-28	15.98	0.78
C-9	47.27	1.61	C-19	23.99	0.95	C-29	28.87	0.96
C-10	36.86	-	C-20	31.61	2.43	C-30	22.61	1.038

One of three compounds was characterized with NMR (^1H , ^{13}C NMR, DEPT, ^1H - ^1H COSY, HMQC, HMBC, and NOE) and demonstrated to be protosta-13(17),24-dien-3 β -ol (Fig. 3-6) based on the following data. The ^1H NMR spectra showed one olefinic proton (δ 5.054) and seven methyl singlets (δ 1.648, 1.541, 1.038, 0.959, 0.945, 0.919, 0.785) as well as one methyl doublet (δ 0.932, d, $J = 6.89\text{Hz}$, 3H). The 150 MHz ^{13}C NMR spectrum revealed the presence of one tertiary-quaternary ($\delta = 125.00$, 130.94 ppm) and one quaternary-quaternary substituted double bond ($\delta = 135.30$, 139.02 ppm). The HMQC spectrum showed that the methyl doublet proton at $\delta = 0.932$ are attached to the carbon at 20.05 ppm, the

methane proton at δ 2.440 is attached to the carbon at 31.607 ppm (C-20), while the methylene proton at δ 2.346 and 1.788 are attached to the carbon at 23.29 ppm (C-12). In the ^1H - ^1H COSY and HMQC spectra, the methylene proton at δ 1.263 show connectivity with two methylene proton at δ 1.760~1.827 and the methane proton at δ 2.440, which are attached to carbons at 26.36 ppm (C-23) and 31.61 ppm (C-20), respectively. In the HMQC spectrum, the δ 2.440 methine proton is coupled by 2J connectivity to carbons at 139.02 ppm (C-13), 28.70ppm (C-16), and 26.36 ppm (C-23). The HMBC also established that the tertiary vinylic proton (δ 5.054) is coupled by 2J to carbons at 130.94 ppm (C-25) and 26.36 ppm (C-23), as well as by 3J connectivity to carbons at 25.71 ppm (C-26), 17.59 ppm (C-27), and 35.68 ppm (C-22). These correlations unambiguously establish key structural features of the two double bonds located between C-13 and C-17, and C-24 and C-25, respectively. further, the presence of NOEs among Me-28/Me-19, Me-19/H-9, H9/Me-18, Me-29/H-3, and H-3/H-5 as well as the absence of NOEs between Me-19/Me-30 and Me-18/Me-30, confirm the trans-syn-trans stereochemistry and the structure as protosta-13(17),24-dien-3 β -ol, a product with $\Delta^{13(17),24}$ double bonds.

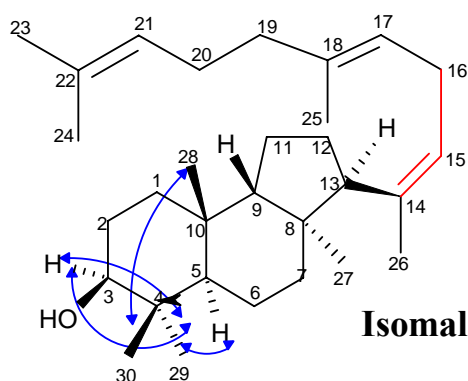
The fifth distinct product was identified to be protosta-17(20),24-dien-3 β -ol (Fig. 3-7), a tetracyclic product with $\Delta^{17(20),24}$ double bonds. The compound showed ^1H NMR spectrum with one olefinic proton (δ 5.084), three vinylic methyl singlets (δ 1.658, 1.579, and 1.553), and five methyl singlets (δ 1.105, 0.933, 0.844, 0.836, and 0.729). The ^{13}C NMR showed the presence of one tertiary-quaternary and one quaternary-quaternary substituted double bonds (δ = 124.68, 131.13 and 126.36, 136.69). These results indicated the presence of tetracyclic nucleus with a terminal hydrocarbon side chain double bond. Correlations of the HMQC, HMBC, and NOE spectra showed the following features: (1) the olefinic proton at δ 5.084 (δ_c 124.68,

C-24) is coupled to carbons at 25.75 ppm (C-26), 17.67 ppm (C-27), 28.05 ppm (C-23), and 33.69 ppm (C-22); (2) the vinylic methyl protons at δ 1.553 (δ_c 20.81, C-21) is coupled to carbons at 126.36 ppm (C-20), 136.69 ppm (C-17), and 33.69 ppm (C-22); (3) the carbon at 33.69 ppm is coupled to protons at δ 1.553 (δ_c 20.81, C-21), 2.063 (δ_c 28.05, C-23), 5.084 (δ_c 124.68, C-24); (4) clear NOE peaks of Me-28/Me-19, H-3/Me-29, Me-29/H-5, Me-19/H-9, H-9/Me-14, and Me-30/H-13, as well as the absence of Me-19/H-5, Me-18/Me-30, and Me-30/H-9 NOE peaks were noticed, thus confirming structure assignment including the stereochemistry and the exocyclic double bond position.



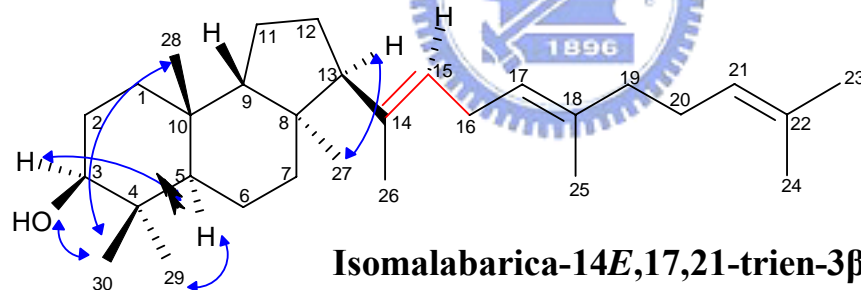
Protosta-17(20),24-dien-3 β -ol (Fig. 3-8)

	^{13}C (δ)	^1H (δ)		^{13}C (δ)	^1H (δ)		^{13}C (δ)	^1H (δ)
C-1	32.6	1.40,1.47	C-11	22.88	1.23,1.48	C-21	20.81	1.56
C-2	25.25	1.62,1.71	C-12	27.2	2.12,1.34	C-22	33.69	2.05
C-3	81.1	4.49	C-13	46.75	2.27,2.29	C-23	28.04	2.02,2.06
C-4	38.18	-	C-14	38.81	-	C-24	124.675	5.08
C-5	47.63	1.54	C-15	30.28	1.10,1.48	C-25	131.13	-
C-6	18.2	1.18,1.50	C-16	29.24	2.03~2.13	C-26	25.75	1.66
C-7	34.56	1.18,1.93	C-17	136.69	-	C-27	17.66	1.58
C-8	50.57	-	C-18	21.66	1.05	C-28	29	0.835
C-9	45.33	1.49	C-19	22.63	0.93	C-29	17.13	0.84
C-10	36.61	0.93	C-20	126.36	-	C-30	16.92	0.73



Isomalabarica-14Z,17,21-trien-3 β -ol (Fig. 3-9)

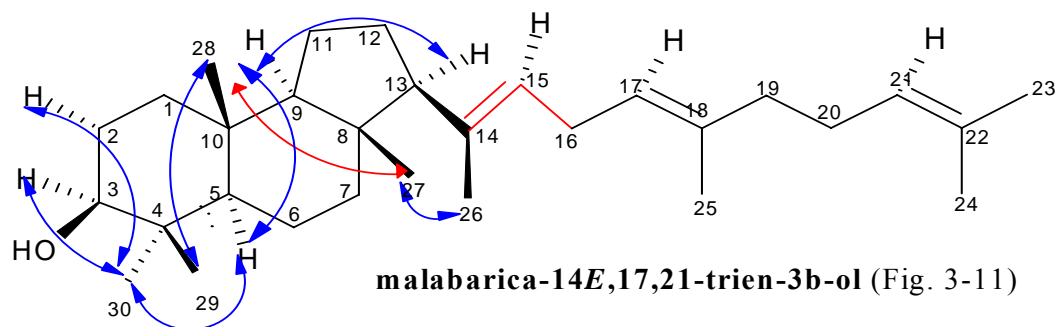
	^{13}C (δ)	^1H (δ)		^{13}C (δ)	^1H (δ)		^{13}C (δ)	^1H (δ)
C-1	33.81	1.449,1.38	C-11	21.16	1.44,1.56	C-21	124.33	5.06
C-2	29.16	1.72,1.62	C-12	25.26	1.86,1.547	C-22	131.32	-
C-3	79.52	3.2	C-13	50.75	2.62	C-23	25.68	1.657
C-4	39.07	-	C-14	137.8	-	C-24	17.66	1.577
C-5	47.63	1.485	C-15	126.76	5.18	C-25	16.11	1.583
C-6	18.79	1.53,1.26	C-16	26.92	2.572	C-26	22.21	1.599
C-7	32.49	1.75,1.17	C-17	123.29	5.03	C-27	29.93	1.072
C-8	44.15	1.072	C-18	134.76	-	C-28	23.09	0.917
C-9	54.41	1.563	C-19	39.66	2.06,1.96	C-29	29.1	0.964
C-10	35.64	-	C-20	26.7	2.06,1.96	C-30	15.93	0.763



Isomalabarica-14E,17,21-trien-3 β -ol (Fig. 3-10)

	^{13}C (δ)	^1H (δ)		^{13}C (δ)	^1H (δ)		^{13}C (δ)	^1H (δ)
C-1	34.11	1.373,1.389	C-11	20.89	1.373,1.526	C-21	124.33	5.07
C-2	29.16	1.75,1.62	C-12	29.91	1.875,1.53	C-22	131.29	-
C-3	79.52	3.23	C-13	59.51	2.046	C-23	1.65	1.577
C-4	39.06	-	C-14	139.156	-	C-24	25.66	1.657
C-5	47.02	1.511	C-15	124.96	4.99	C-25	16.09	1.6
C-6	18.62	1.21,1.53	C-16	29.99	2.68	C-26	18.08	1.548
C-7	32.14	1.62,1.18	C-17	123.29	5.09	C-27	29.74	1.04
C-8	44.51	1.04	C-18	134.94	-	C-28	23.14	0.91
C-9	52.95	1.51	C-19	39.65	2.06,1.96	C-29	29.08	0.954
C-10	35.37	-	C-20	26.75	2.06,1.96	C-30	15.91	0.753

A third novel compound, unknown A, isolated from the ERG7^{F699M} mutant was proposed to be malabarica-14*E*,17*E*,21-trien-3 β -ol, a chair-chair (C-C) 6-6 -5 tricyclic product with trans-anti-trans stereochemistry and $\Delta^{14,17,21}$ double bonds. First, the compound showed ¹H NMR spectrum with four vinylic methyl singlets (δ 1.64, 1.651, 1.661 and 1.712), and four methyl singlets (δ 0.664, 0.809, 0.879, and 0.997), and three double bond protons (δ 5.15, 5.162, and 5.165). Second, the ¹³C NMR showed the presence of three tertiary-quaternary (δ = 124.53, 134.66, 123.625, 134.958, and 124.467, 131.408). These results indicate the presence of tricyclic nucleus with a terminal hydrocarbon side chain double bond. Correlations of the HMQC, HMBC, and NOE spectra showed the following features: (1) the vinyl proton at δ 5.16 (δ_c 124.53, C-15) is coupled to carbons at 27.144 ppm (C-16), 123.625 ppm (C-17), 59.94 ppm (C-13), and 18.102 ppm (C-26); (2) the vinyl protons at δ 5.15 (δ_c 123.625, C-17) is coupled to carbons at 27.144 ppm (C-16), 15.91 ppm (C-25), and 39.84 ppm (C-19); (3) the vinyl protons at δ 5.162 (δ_c 124.467, C-21) is coupled to carbons at 25.555 ppm (C-23) and 17.54 ppm (C-24); (4) the proton at δ 2.76 (δ_c 27.144, C-16) is coupled to carbons at 134.66 ppm (C-14), 124.53 ppm (C-15), 123.625 ppm (C-17), and 134.958 ppm (C-18); (5) the proton at δ 2.021 (δ_c 59.94, C-13) is coupled to carbons at 24.37 ppm (C-12), 134.66 ppm (C-14), 44.02 ppm (C-8), 62.96 ppm (C-9) and 18.102 ppm (C-26); These correlations established the bond connectivity between the tricyclic nucleus skeleton and the exocyclic hydrocarbon side chain as well as the double bond positions. The distinct evidence of NOE spectra was observed among Me-28/Me-29, Me28/Me-27, H-5/H-9, and H-9/H-13 which confirmed the presence of trans-anti-trans ring junction of the malabaricane nucleus. Because of the scanty amount and purity of unknown A, we still needed to culture the large amount of ERG7^{F699M} mutant and confirm the stereochemistry for this trans-anti-trans structure.



	¹³ C (δ)	¹ H(δ)		¹³ C (δ)	¹ H(δ)		¹³ C (δ)	¹ H(δ)
C-1	38.54	1.08,1.511	C-11	19.70	1.42,1.515	C-21	124.467	5.162
C-2	27.46	1.615~1.655	C-12	24.37	1.833,1.61	C-22	131.408	-
C-3	79.23	3.22	C-13	59.94	2.02	C-23	25.55	1.71
C-4	38.836	-	C-14	134.66	-	C-24	17.54	1.64
C-5	56.46	0.852,0.831	C-15	124.53	5.16	C-25	15.91	1.661
C-6	19.36	1.485,1.62	C-16	27.144	2.76	C-26	18.10	1.651
C-7	41.239	1.51,1.82	C-17	123.625	5.15	C-27	15.06	0.664
C-8	44.02	-	C-18	134.958	-	C-28	15.37	0.879
C-9	62.96	1.244	C-19	39.84	2.02	C-29	15.191	0.809
C-10	36.977	-	C-20	26.883	2.11	C-30	28.06	0.997

Table 7 showed the product profile produced by the ERG7^{F699X} site-saturated mutants. Among the inviable mutants, no new product was produced except for the ERG7^{F699N} and ERG7^{F699K} mutants. These two mutants grew on ergosterol medium more slowly than the wild type cells and produced a similar ratio of product profiles except for unknown B. For the viable mutants, the ERG7^{F699L}, ERG7^{F699I}, and ERG7^{F699P} mutants produced lanosterol as sole product whereas the ERG7^{F699H} mutant produced the protosta-13(17),24-dien-3β-ol, protosta-17(20),24-dien-3β-ol and lanosterol in the relative ratio of 70:17:13. To our surprise, the ERG7^{F699M} mutant generated all kinds of the product profiles from the site-saturated mutants of ERG7^{F699X}, including protosta-13(17),24-dien-3β-ol, protosta-17(20),24-dien-3β-ol, malabarica-14*E*,17*E*,21-trien-3β-ol and unknown A. Notably, the protosta-13(17),24-dien-3β-ol was generated as the major compound with lanosterol at the level <0.2% from the ERG7^{F699T} mutant.

Table 7. The ratio of product profiles from *Sce*ERG7^{F699X} mutants.

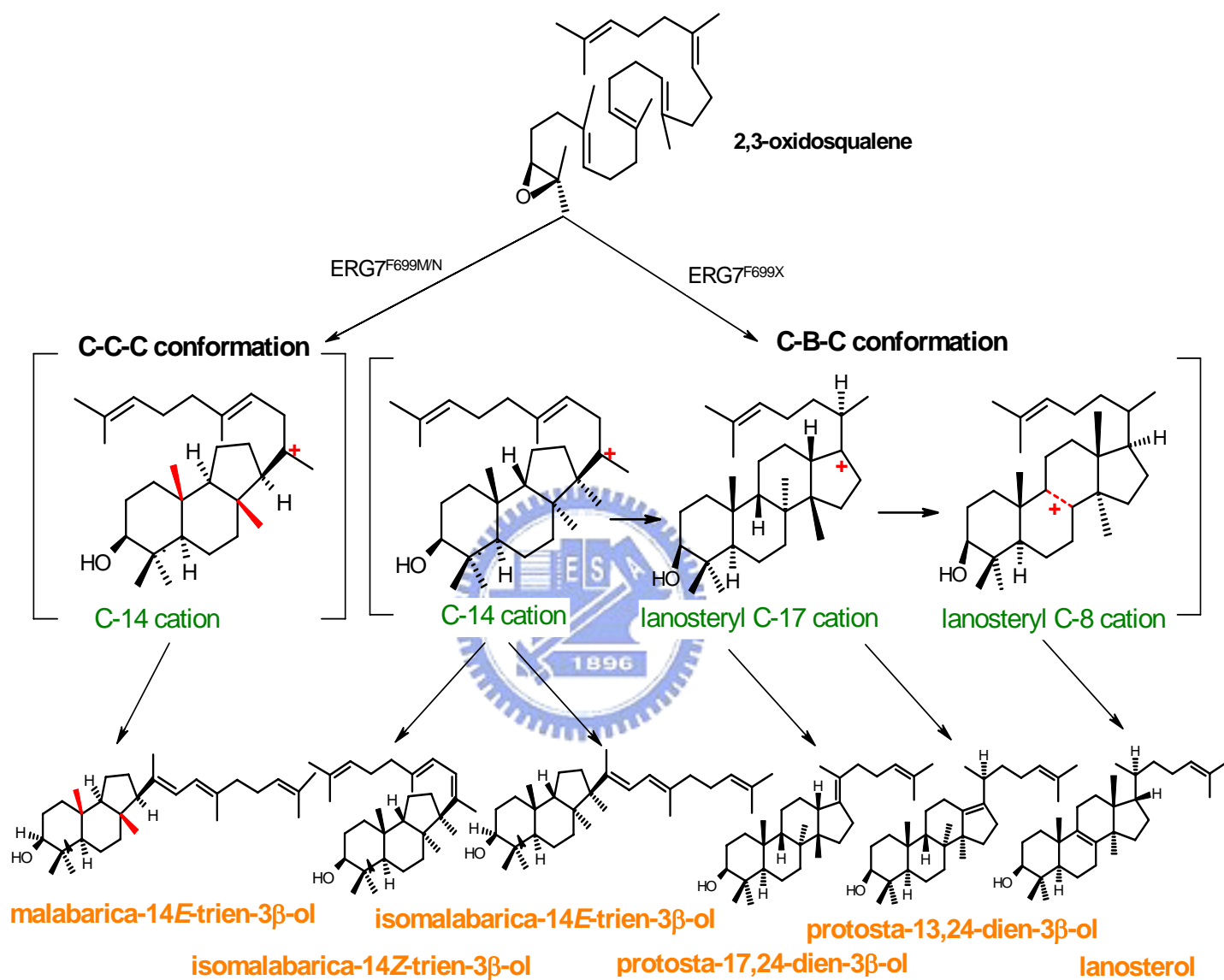
Substitution of Phe699	No products	Isomalabarica-14E	Isomalabarica-14Z	LA	13,17-LA	17,20-LA	Malabarica-14E	Unknown A
Gly	v							
Ala	v							
Val	v							
Leu				100				
Ile				100				
Asp	v							
Asn					62	12	6	20
Glu	v							
Gln	v							
His				13	70	17		
Lys					63	17		20
Arg	v							
Ser	v							
Thr				1	99			
Cys	v							
Met		17	18	1	46	10	7	1
Tyr	v							
Trp	v							
Pro				100				

Scheme IV showed the proposed cyclization/rearrangement pathway occurred in the ERG7^{F699X} site-saturated mutants. In the Phe699 mutations except for the Asn and Met of substitutions, the oxidosqualene prefolded in chair-boat-chair conformation when entering the active site cavity of enzyme. In the ERG7^{F699N} and ERG7^{F699M} mutants, the minor part of substrate might enforce chair-chair-chair conformation by the different interactions from the location of the substituted amino acid residue. In one way, the C-C-C substrate was cyclized to a tricyclic Markonikov C-14 cation that directly attracted C-15 proton to yield malabarica-14Z,17E,21-trien-3 β -ol as end

product. Alternatively, the C-B-C substrate conformer was cationic cyclized to a similar tricyclic cation as the first stopping point. Possibly, the substrate is converted into the prosteryl C-20 cation after C-ring expansion and subsequent D-ring annulations. Then, a backbone rearrangement of H-17 α to H-20 α *via* 1,2 hydride shift, generated the lanosteryl C-17 cation. Elimination of proton originally at C-13 or after hydride shift from H-17 α to H-20 α yielded protosta-13(17),24-dien-3 β -ol and protosta-17(20),24-dien-3 β -ol as end product, respectively. Finally, skeletal rearrangement of two methyl groups would generate the lanosteryl C-8 cation, which undergoes deprotonated to form lanosterol.

Among these products derived from the ERG7^{F699X} mutants, including protosta-13(17),24-dien-3 β -ol and protosta-17(20),24-dien-3 β -ol, indicated that the premature deprotonations of the rearrangement reactions were occurred at lanosteryl C-17 cation. The formation of truncated cyclization intermediates by the Phe to Met mutant of ERG7 suggests that Phe699 might also play a crucial role both in influencing substrate prefolding and tricyclic cation stabilization, in addition to stabilize rearrangement cation. The isolation of malabarica-14Z,17E,21-trien-3 β -ol from the ERG7^{F699M} mutant suggested a conformational change of the substrate from chair-boat-chair to chair-chair-chair prefolded conformation. This finding supports that the plasticity and diversity of products from the ERG7 mutant enzyme in changing the active site structure and subsequent reaction pathway.

Scheme IV. Proposed cyclization/rearrangement pathway of oxidosqualene in TKW14C2 expressing ERG7^{Y699X} site-saturated mutagenesis.



There were many possible reasons for the production of the diverse product profiles from ERG7^{F699M} mutant. However, we provided one explanation as follows. The structure comparison between ERG7 and SHC showed that β -sheep domain of the ERG7^{G697-C703} region was more loosely packed than the corresponding region within SHC. Compared with the sequence of SHC, a one-residue deletion between Gly697 and Val698 of ERG7 was observed. The results from the product profile indicated that the position of Phe699 was oriented to stabilize the lanosteryl C-17 cation intermediate, Thorma *et al.* have proposed that the Phe699 side chain was positioned to stabilize the anti-Markovnikov secondary cation created at C-13 during C-ring formation (lanosterol numbering). Perhaps the substitution of Phe699 with Met might cause the inappropriate position of the residue and subsequently disorder the enzyme structure in part, thus allowed the unconstrained motion of the substrate. Alternatively, the ERG7^{F699M} mutation might affect substrate folding and cyclization to truncated tricyclic products through partial disruption of transient dipole interactions between carbocation intermediate and the hydroxyl group of Tyr99. However, other factors, including the steric or electrostatic effect might be involved in the substrate folding and diverse product profiles.

Chapter 4 Discussion and Conclusion

A “site-saturated mutagenesis” approach was the replacement of the target residue with each other of the proteinogenic amino acids. This technique was agreed to make a detailed understanding of the effects, both steric and electrostatic, of the other amino acids, substituted at the positions of target. In conclusion, the Tyr510 and Phe699 within oxidosqualene cyclase from *Saccharomyces cerevisias* were site-saturated mutated to analyze the functional role and catalytic mechanism of these highly conserved aromatic acid residues in active site cavity of cyclases.

In the part of *Sce*ERG7^{Y510X} mutants:

1. We have constructed the saturated mutants of ERG7^{Y510} from *Saccharomyces cerevisiae* and analyzed all of them by the ergosterol complement selection and GC-MS. Among the viable mutants, the Tyr510Lys, Tyr510Arg, Tyr510Thr, Tyr510Pro and Tyr510Trp mutations failed to complement the function of cyclization. The finding suggested that the different side chain substitution of Tyr510 might influence the enzyme stability, and/or abolish catalytic activity.
2. The Tyr510 of *S.cerevisiae* ERG7 corresponds to Tyr420 in *A.acidocaldarius* SHC and to Tyr532 in *A.thaliana* CAS. The replacement of tyrosine in *Sce*ERG7 with other proteinogenic amino acids resulted in a mixture of monocyclic achilleol A, tricyclic (13 α H)-isomalabarica-14(26),17,21-trien-3 β -ol and two tetracycles, lanosterol and parkeol. The truncated and altered deprotonation products from mutants supported an evidence of the aromatic hypothesis for the lanosterol biosynthesis. The tricycle, (13 α H)-isomalabarica-14(26),17,21-trien-3 β -ol,

was described as an intermediate for directly trapping of the C-B 6-6-5 Markovnikov cation in the oxidosqualene cyclization/rearrangement reactions.

3. By the human OSC crystal structure, the phenolic group of Tyr510 was hydrogen bonded to the proposed active site base His234. The proximity of the phenolic oxygen to the C9 proton suggested that Tyr510 was the initial proton acceptor and transfers its phenolic proton to His234. On the other hand, the Tyr510 mutants might alter the final deprotonation step by substituting the hydrogen-bond network between His234 and Tyr510 in the cyclization/rearrangement cascades.
4. In order to clarify the relationships of the product profiles ratios between the $ERG7^{Y510X}$ and $ERG7^{H234X}$ mutants, the double site-specified mutagenesis of Tyr510 and His234 residues was performed to identify the steric influence on residues located at active site. The preliminary result of $ERG7^{H234W/Y510W}$ and $ERG7^{H234W/Y510V}$ mutants showed that the polycyclic products, lanosterol in $ERG7^{H234W/Y510V}$ mutant but not in $ERG7^{H234W/Y510W}$ mutant. The explanation might be described due to the steric and electrostatic effects on the stereochemistry of these amino acid residues within OSC.

In the part of *Sce*ERG7^{F699X} mutants:

1. The result of site-saturated $ERG7^{F699X}$ mutants provided strong support for the functional role of Phe699 in influencing the prefolded substrate conformation and its further propagation in the cyclization/rearrangement reactions. Thoma *et al.* suggested that the Phe696 (corresponding to Phe699 in *S. cerevisiae* ERG7) close to the D-ring of lanosterol was positioned to stabilize the lanosteryl C-14 cation. However, our research implied that the position on

Phe699 might stabilize the carbonic intermediate at C-17 but not C-14. The difference of them might be possibly dependent on the species diversity.

2. The product, protosta-13,24-dien-3 β -ol, was observed as a major product of the mutants, especially in ERG7^{F699T} mutant. Mutant that showed a complete change in product specificity from lanosterol formation or protosta-17(20),24-dien-3 β -ol to protosta-13(17),24-dien-3 β -ol could be affected under *in vivo* or *in vitro* experiment. This finding might explain that the protosta-13(17),24-dien-3 β -ol was more appropriate substrate than protosta-17(20),24-dien-3 β -ol or lanosterol in metabolism pathway.
3. The isolation of (13 α H)-isomalabarica-14(15)Z-17,21-trien-3 β -ol and (13 α H)-isomalabarica-14(15)E-17,21-trien-3 β -ol from ERG7^{F699M} provided support for the hypothesis that formation of lanosterol from oxidosqualene in ERG7-catalyzed cyclization/rearrangement reaction proceeded *via* the Markovnikov C-B 6-6-5 tricyclic cation. Interestingly, both of isomers were also observed and isolated from *ScE*ERG7^{Y99X} mutants. Moreover, the residue Phe699 is neighbored to Tyr99 in the homology structure model. Taken together, these results demonstrated the functional role of the ERG7^{Phe699} residue in influencing Markovnikov tricyclic C-14 and lanosteryl C-17 cations stabilization as well as the plasticity of the ERG7 mutant enzyme in changing the active site structure and subsequent reaction cascade.
4. This is the first example in which the substrate conformation could be successfully altered from chair-boat-chair to chair-chair-chair by a single amino acid mutation of the ERG7 enzyme. In addition, the replacement of Phe with Thr resulted in a complete change from lanosterol to protosta-13(17),24-dien-3 β -ol, which represented the best known of ERG7 mutated to make truncated or rearranged product. Finally, the experimental

results confirmed our working hypothesis and coupled with site-saturated mutagenesis and product characterization in the validation of the structure-reactivity relationships where individual approach would not be achieved.



Chapter 5 Future Work

First, according to the truncated products from the $ERG7^{F699X}$ mutants, we suppose that the unknown A might be protosta-16(17),24-dien-3 β -ol, the ultimate compound for deprotonating at lanosterol C-17 cation intermediate. However, the isolation and characterization of unknown A compound in *S. cerevisiae* $ERG7^{F699M}$ mutants will be continue for deeply understanding of functional role of Phe699 of $ERG7$ enzyme. Second, in order to quantify the real amount of the metabolite in the TKW14C2, we will make the $ERG1/ERG11$ double knockout with TKW14C2 for the in vitro assay. $ERG1$ encodes squalene monooxygenase (also called squalene epoxidase), an enzyme that oxidizes squalene to form squalene 2,3-epoxide. $ERG11$ encodes lanosterol 14- α -demethylase, an enzyme catalyzes the C-14 demethylation of lanosterol to form 4,4'-dimethyl cholesta-8,14,24-triene-3-beta-ol. Both of $ERG1$ and $ERG11$ are essential in the ergosterol biosynthesis and the disruptions of oxidosqualene formation, lanosterol formation, and the subsequent reactions from $ERG1/ERG7/ERG11$ triple-knock-out strain, we would calculate the relative amount of products to the exogenous oxidosqualene supplement. Finally, the intermediates isolated from $ERG7^{F699X}$ mutants, including the alternative deprotonation and the truncated products might be used as candidates for drug screening system in the future.

Reference

- 1 N. Nagata and M. Suzuki, *Planta* 216, 345 (2002).
- 2 R. Xu, G. C. Fazio, and S. P. T. Matsuda, *Phytochemistry* 65 (3), 261 (2004).
- 3 T. Martin, S. E. Parker, and R. Hedstrom et al., *Hum Gene Ther* 10 (5), 759 (1999).
- 4 E. J. Corey, S. C. Virgil, and S. Sarshar, *J. Am. Chem. Soc.* 113, 8171 (1991).
- 5 I. Abe and G. D. Prestwich, *J Biol Chem* 269 (2), 802 (1994).
- 6 E. J. Corey, H. Cheng, and C. H. Baker et al., *J. Am. Chem. Soc.* 119, 1277 (1997).
- 7 W. S. Johnson, S. J. Telfer, and S. Cheng et al., *J. Am. Chem. Soc.* 109, 2517 (1987).
- 8 R. J. Griffin and M. F. Stevens, *Anticancer Drug Des* 7 (6), 443 (1992).
- 9 E. J. Corey and S. C. Virgil, *J. Am. Chem. Soc.* 113, 4025 (1991).
- 10 T. Merkofer, K. U. Wendt, and M. Rohmer, *Tetrahedron letters* 40, 2121 (1999).
- 11 T. S. Gasch and M. Stahl, *J Comput Chem* 24 (6), 741 (2003).
- 12 V. Q. Huneus, M. H. Wiley, and M. D. Siperstein, *Proc Natl Acad Sci U S A* 76 (10), 5056 (1979).
- 13 I. Abe, M. Bai, X. Y. Xiao et al., *Biochem Biophys Res Commun* 187 (1), 32 (1992).
- 14 E. J. Corey, S. P. T. Matsuda, C. H. Baker et al., *Biochem Biophys Res Commun* 219 (2), 327 (1996).
- 15 T. K. Wu, Y. T. Liu, and C. H. Chang, *Chembiochem* 6 (7), 1177 (2005).
- 16 T. K. Wu, Y. T. Liu, F. H. Chiu et al., *Org Lett* 8 (21), 4691 (2006).

- 17 E. E. Van Tamelen, J. Willet, M. Schwartz et al., *J. Am. Chem. Soc.* 88 (24),
5937 (1966).
- 18 E. J. Corey, C. H. Baker, H. Cheng, S. P. T. Matsuda et al., *J. Am. Chem. Soc.*
119, 1289 (1997).
- 19 E. J. Corey and D. D. Staas, *J. Am. Chem. Soc.* 120, 3526 (1998).
- 20 W. S. Johnson, S. D. Lindell, and J. Steele, *J. Am. Chem. Soc.* 109, 5852
(1987).
- 21 I. Abe, M. Rohmer, and G. Prestwich, *Chem. Rev.* 93, 2189 (1993).
- 22 I. Abe, Y. F. Zheng, and G. D. Prestwich, *Biochemistry* 37 (17), 5779 (1998).
- 23 T. K. Wu, M. T. Yu, Y. T. Liu et al., *Org Lett* 8 (7), 1319 (2006).
- 24 T. K. Wu, Y. T. Liu, C. H. Chang et al., *J Am Chem. Soc.* 128 (19), 6414
(2006).
- 25 S. Lodeiro and S. P. T. Matsuda, *Org Lett* 8, 439 (2006).
- 26 R. Thoma, T. Schulz-Gasch, B. D'Arcy et al., *Nature* 432 (7013), 118 (2004).
- 27 J. C. Sacchettini and C. D. Poulter, *Science* 277 (5333), 1788 (1997).
- 28 H. S. Robinson, *J Natl Med Assoc* 62 (6), 474 (1970).
- 29 B. J.robustell, I. Abe, and G. D. prestwich, *Tetrahedron letters* 39, 9385 (1998).
- 30 M. J. R. Segura and S. P. T. Matsuda, *Nat Prod Rep* 20, 304 (2002).
- 31 H. H. Rees, L. J. Goad, and T. W. Goodwin, *Biochemistry* 107, 417 (1968).
- 32 S. Lodeiro, M. J. Segura, M. Stahl et al., *Chembiochem* 5 (11), 1581 (2004).
- 33 E. A. Hart, L. Hua, and S. P. T. Matsuda, *J. Am. Chem. Soc.* 121, 9887 (1999)
- 34 T. K. Wu and J. H. Griffin, *Biochemistry* 41 (26), 8238 (2002).
- 35 W. K. Wilson, B. Jennifer, R. Herrera, and S. P. T. Matsuda, *J. Am. Chem. Soc.*
122, 6765 (2000).
- 36 M. M. Meyer and SPT. Matsuda, *Org Lett* 4, 1395 (2002).
- 37 T. Dang, I. Abe, and Y. F. Zheng et al., *Chem Biol* 6 (6), 333 (1999).

- 38 M. J. Segura, B. E. Jackson, and S. P. T. Matsuda, *Nat Prod Rep* 20 (3), 304
(2003).
- 39 K. U. Wendt, K. Poralla, and G. E. Schulz, *Science* 277 (5333), 1811 (1997).
- 40 M. Rohmer and K. Proalla, *Tetrahedron letters* 40, 6009 (1999).
- 41 D. W. Chirstianson, *Chem. Rev.* 106 (8), 3412 (2006).
- 42 T. Sato and T. Hoshino, *Chem. Commun*, 2617 (1998).
- 43 T. Hoshino, *Biosci. Biotechnol. Biochem* 63, 2038 (1999).
- 44 C. J. Buntel and J. H. Griffin, *J. Am. Chem. Soc.* 114, 9711 (1992).
- 45 S. P. T. Matsuda, L. B. Darr, E. A. Hart et al., *Org Lett* 2 (15), 2261 (2000).

